Published in final edited form as:
J Neurochem. 2008 January ; 104(2): 336–352. doi:10.1111/j.1471-4159.2007.04971.x.

Differential distribution of proteins and lipids in detergent-resistant and detergent-soluble domains in rod outer segment plasma membranes and disks

Michael H. Elliott[*,1], **Zack A. Nash**[†,1], **Nobuaki Takemori**[‡], **Steven J. Fliesler**[§], **Mark E. McClellan**[*], and **Muna I. Naash**[†]

[*] Department of Ophthalmology, University of Oklahoma Health Sciences Center, Oklahoma City, Oklahoma, USA

[†] Department of Cell Biology, University of Oklahoma Health Sciences Center, Oklahoma City, Oklahoma, USA

[‡] Department of Biochemistry and Molecular Biology, University of Oklahoma Health Sciences Center, Oklahoma City, Oklahoma, USA

[§] Departments of Ophthalmology and Pharmacological & Physiological Science, Saint Louis University School of Medicine, St Louis, Missouri, USA

Abstract

Membrane heterogeneity plays a significant role in regulating signal transduction and other cellular activities. We examined the protein and lipid components associated with the detergent-resistant membrane (DRM) fractions from retinal rod outer segment (ROS) disk and plasma membrane-enriched preparations. Proteomics and correlative western blot analysis revealed the presence of α and β subunits of the rod cGMP-gated ion channel and glucose transporter type 1, among other proteins. The glucose transporter was present exclusively in ROS plasma membrane (not disks) and was highly enriched in DRMs, as was the cGMP-gated channel β-subunit. In contrast, the majority of rod opsin and ATP-binding cassette transporter A4 was localized to detergent-soluble domains in disks. As expected, the cholesterol: fatty acid mole ratio was higher in DRMs than in the corresponding parent membranes (disk and plasma membranes, respectively) and was also higher in disks compared to plasma membranes. Furthermore, the ratio of saturated: polyunsaturated fatty acids was also higher in DRMs compared to their respective parent membranes (disk and plasma membranes). These results confirm that DRMs prepared from both disks and plasma membranes are enriched in cholesterol and in saturated fatty acids compared to their parent membranes. The dominant fatty acids in DRMs were 16: 0 and 18: 0; 22: 6n3 and 18: 1 levels were threefold higher and twofold lower, respectively, in disk-derived DRMs compared to plasma membrane-derived DRMs. We estimate, based on fatty acid recovery that DRMs account for only ~ 8% of disks and ~ 12% of ROS plasma membrane.

Keywords

cholesterol; detergent-resistant membranes; fatty acids; membrane microdomains; photoreceptor; proteomics; raft

Address correspondence and reprint requests to Muna I. Naash, PhD, University of Oklahoma Health Sciences Center, 940 Stanton L. Young Blvd., BMSB 781, Oklahoma City, OK 73104, USA., muna-naash@ouhsc.edu.

[1]These authors contributed equally to this work.

Cellular membranes display lateral heterogeneity within the two-dimensional plane of the bilayer and contain specific lipid species organized into discrete membrane microdomains [reviewed in (Simons and Ikonen 1997; Pike 2003; Laude and Prior 2004; Jacobson *et al.* 2007)]. These microdomains are of relatively low fluidity and high order and are enriched in cholesterol, sphingolipids, and lipids with saturated fatty acyl chains, relative to bulk phase membrane lipids [reviewed in (Brown and London 2000; Pike 2004; Simons and Vaz 2004; Brown 2006)]. Presumably because of tight fatty acyl chain packing, these membrane domains are relatively resistant to extraction with cold non-ionic detergents (e.g., Triton X-100) and exhibit low buoyant density upon density-gradient ultracentrifugation (Brown and Rose 1992; Brown and London 2000; Pike *et al.* 2002; Pike 2003; Schuck *et al.* 2003; Simons and Vaz 2004). Proteins differentially associate with lipid microdomains depending upon various factors, including the specific lipid composition of rafts and the nature of lipid moieties attached to the proteins (Resh 1999; Zacharias *et al.* 2002; Kusumi and Suzuki 2005). Thus, membrane domains may act as organizing centers to transiently compartmentalize membrane components with specific cohorts of other molecules (e.g., signaling proteins) to facilitate their function within specific regions of the plasma membrane (PM) [reviewed in (Simons and Ikonen 1997; Isshiki and Anderson 2003; Pike 2006; Allen *et al.* 2007)].

Vertebrate phototransduction involves a prototypical G protein-coupled cascade in which the photo-activated receptor, rhodopsin, promotes guanine nucleotide exchange by the heterotrimeric G protein, transducin (Tαβγ), resulting in activation of the effector, cGMP-phosphodiesterase (PDE6), thereby modulating cyclic nucleotide-gated (CNG) ion channel conductance by reducing cGMP concentration [reviewed in (Arshavsky *et al.* 2002; Ridge *et al.* 2003; Chen 2005; Zhang and Cote 2005)]. In rod cells, photo-transduction occurs within the rod outer segment (ROS), an organelle containing two separate membrane systems: (i) densely packed stacks of disk membranes enriched in rhodopsin, and (ii) a surrounding PM containing the CNG ion channel (Molday and Molday 1987; Molday 1998). The existence of cholesterol-enriched membrane microdomains in photoreceptor PM and disks was proposed over 25 years ago following the observation, in freeze fracture replicas, of particle-free patches (PFPs) that preferentially localized the cholesterol-binding antibiotic, filipin, in ROS PM and in the basal disks of both frogs and mice (Andrews and Cohen 1979). More recently, raft-like domains have also been reported in native, unfixed disks by atomic force microscopy (Liang *et al.* 2003; Fotiadis *et al.* 2004). Further support for the presence of membrane domains in ROS was provided when Seno *et al.* (Seno *et al.* 2001) first prepared detergent-resistant membrane (DRMs) from bovine ROS. Subsequent studies of ROS-derived DRMs indicate the association of several proteins involved in phototransduction (Seno *et al.* 2001; Nair *et al.* 2002, 2004; Elliott *et al.* 2003; Liu *et al.* 2003; Senin *et al.* 2004) and in the maintenance of ROS structure (Maw *et al.* 2000; Roper *et al.* 2000; Boesze-Battaglia *et al.* 2002) with DRM fractions.

Interestingly, most of the proteins identified in ROS-derived DRMs are either integrally or functionally associated with disk membranes [e.g., rod opsin, transducin (Seno *et al.* 2001), guanylate cyclase, arrestin, (Nair *et al.* 2002), Rom-1 (Boesze-Battaglia *et al.* 2002), and rhodopsin kinase (Senin *et al.* 2004)]. Although prior studies have not employed proteomics to identify DRM-associated candidate proteins in ROS membranes, this approach has been used by others to determine the proteome of DRMs in other cells and tissues (Foster *et al.* 2003; Keller *et al.* 2004; Li *et al.* 2004; Wollscheid *et al.* 2004; Yu *et al.* 2005; Gupta *et al.* 2006; Le Naour *et al.* 2006).

To gain insight into the potential role of raft domains in photoreceptors, we employed proteomic analysis to identify ROS-derived, DRM-associated proteins. Using this approach in conjunction with western blot analysis, several proteins heretofore not known to be DRM-associated were identified and their relative distributions within DRM fractions were evaluated.

From this analysis, we report the dramatic enrichment of CNGβ-1 and Glut-1 in DRM fractions, two proteins that are integral to the ROS PM (Cook *et al.* 1989; Hsu and Molday 1991). In contrast, rod opsin and ATP-binding cassette protein A4 [ABCA4, or ABCR; (Sun and Nathans 2001; Kaminski *et al.* 2006)] are preferentially associated with the detergent-soluble bulk phase fraction of the disks. Our analysis of DRMs obtained from disk- and PM-enriched fractions indicates that the overwhelming majority of DRM-localized rod opsin in ROS membranes is derived from disks, not the PM. In addition, we present the first detailed fatty acid compositional analysis of DRMs derived from ROS disk- and PM-enriched membrane fractions, from which we have calculated the relative contributions of each membrane compartment to total ROS-derived DRMs. The results of this study provide direct evidence that DRMs are present in slightly greater amounts in the ROS PM than in the disks (~12% vs. ~8%, respectively). However, as PM represents only ~3% of the total ROS membranes, disks represent the major source of DRMs found in the ROS. Contrary to the prevailing concept that DRMs act as platforms for the organization of signal transduction machinery in cells, our findings are more consistent with a model wherein phototransduction takes place in the non-DRM domains of retinal ROS, whereas DRMs represent a transiently sequestered reservoir of 'transductionally silent' proteins.

Materials and methods

Materials

Polyclonal antibodies to transducin-alpha subunit (Tα) and Glut-1 were purchased from Santa Cruz Biotechnology (Santa Cruz, CA, USA). A polyclonal antibody to Cav-1 was obtained from BD Biosciences (San Jose, CA, USA). Monoclonal antibodies against the vertebrate rod visual pigment rhodopsin (1D4; which also recognizes opsin, the protein moiety without the retinoid chromophore attached), Rom-1 (1C6), ABCA4 (Rim 3F4), CNGβ-1 (PMs5E11), and glutamic acid-rich protein (GARP) (Garp 4B1) were generously provided by Dr. Robert Molday, University of British Columbia. Rabbit polyclonal antibody against residues 331–346 of mouse Rds (Rds-CT) was generated by immunizing rabbits with the corresponding peptides coupled to keyhole limpet hemocyanin (Nour *et al.* 2004). A bicinchonic acid protein assay kit was obtained from Pierce (Rockford, IL, USA). Unless otherwise stated, all other reagents were obtained from Sigma–Aldrich (St Louis, MO, USA).

Preparation of ROS, disk and PM-enriched fractions and DRMs

Rod outer segment membranes were prepared from either fresh (Mikkelson Beef, Inc., Oklahoma City, OK, USA) or frozen (Animal Technologies Inc., Tyler, TX, USA) bovine retinas by discontinuous sucrose density-gradient centrifugation as previously described (Martin *et al.* 2005). In some experiments to isolate disks and PM-enriched fractions, ROS were prepared by continuous sucrose density-gradient centrifugation as previously described (Zimmerman and Godchaux 1982; Elliott *et al.* 2003). In the case of fresh retinas, eyes were refrigerated immediately after slaughter and transported on ice to the laboratory; retinas were then dissected within 6 h of slaughter and ROS were immediately prepared there from. Commercially obtained frozen retinas (harvested by the supplier, individually flash frozen in liquid nitrogen) were shipped to the laboratory on dry ice. Following ROS isolation or disk/PM fractionation by hypotonic lysis and Ficoll flotation, protein content was determined by bicinchonic acid protein assay, using bovine serum albumin (BSA) as a standard. DRMs were either prepared immediately or from previously frozen ROS, disks or PM preparations. We have observed no significant differences in the fractionation of DRM constituents from frozen vs. 'fresh' starting materials (whole retinas or membranes). It should be noted that, in some ROS preparations from frozen retinas, the relative mol% of DHA was significantly reduced (e.g., by up to ~20 mol%) and a concomitant increase in the relative mol% of 22: 5n-6 was observed (data not shown). Based upon previous studies on rodents fed n-3 deficient diets

(Wiegand *et al.* 1991) and after discussion with representatives from Animal Technologies Inc., we suspected that this deviation occurred as a result of dietary changes in cattle (i.e., grass- vs. feed lot-fed). This observation highlights the potential heterogeneity of bovine retina samples. As a result, we excluded such samples from the analyses presented herein.

Disk- and PM-enriched fractions were prepared by hypotonic lysis and centrifugation (80 000 *g*) on 5% (w/v) Ficoll by the method of Smith and Litman (Smith and Litman 1982), with one exception. The original Smith/Litman protocol was designed to isolate osmotically intact disks and the starting material was crude ROS. In our studies, the starting material used was purified ROS (Zimmerman and Godchaux 1982). These 'sealed' (osmotically intact) ROS are well-characterized and contain little contamination from inner segments, RPE, or synaptic vesicles (Elliott *et al.* 2003). Therefore, centrifugation in 5% Ficoll results in a buoyant fraction (accumulating at the Ficoll/water interface) enriched in osmotically intact disks and a pellet enriched in ROS-derived PM.

Detergent-resistant membranes were prepared from intact ROS and from disk- and PM-enriched membranes as previously described (Seno *et al.* 2001; Elliott *et al.* 2003). In brief, purified membrane fractions (3 mg/mL for intact ROS, 2.5 mg/mL for disk and PM fractions, final protein concentration) were solubilized in ice-cold 1% (by vol.) Triton X-100, homogenized by three passes through a 20-guage needle and allowed to incubate for 10 min on ice. As in a previous study (Martin *et al.* 2005), the detergent: lipid molar ratio was determined to be 3: 1 for intact ROS and 3.6: 1 for disk and PM preparations, respectively. We found no significant difference between disk and PM parent membranes with respect to their fatty acids: protein ratio. The solubilized membranes were adjusted to a final sucrose concentration of 0.9 mol/L by the addition of 2.4 mol/L sucrose in Buffer A (10 mmol/L Tris–HCl, pH 7.4, 100 mmol/L NaCl, and 1 mmol/L EDTA), and then overlaid sequentially with 0.75 mol/L, 0.6 mol/L and 0.5 mol/L sucrose (all in buffer A) and centrifuged at 200 000 *g* for 18–20 h at 4°C (Beckman Optima L-80 XP Ultracentrifuge, using a SW60Ti rotor; Beckman Coulter, Inc., Fullerton, CA, USA). Gradient fractions (0.49 mL each) were collected manually from the top to bottom of the gradients. The DRMs were visible as an opaque band at the 0.5–0.6 mol/L sucrose interface. The yield of DRMs based on the recovery of fatty acids compared to parent membranes was 8% and 12% for disk and PM fractions, respectively. We recovered 4.8% and 5.2% of the total protein in DRM fractions from disk and PM, respectively. These recoveries are similar to those we previously reported for DRMs derived from intact ROS (Martin *et al.* 2005).

Proteomic analysis

The DRM-enriched fractions were identified based upon the enrichment of Cav-1 in low-buoyant density fractions on western blots. Cav-1 was used as a raft-associated 'marker' as it is known to be present in ROS-derived DRMs (Boesze-Battaglia *et al.* 2002; Nair *et al.* 2002; Elliott *et al.* 2003; Senin *et al.* 2004; Martin *et al.* 2005). These fractions (fractions 1–4) were pooled and diluted fourfold with Buffer A and centrifuged at 150 000 *g* for 2 h at 4°C in a Sorvall Discovery M150 rotor (S150AT-0148). The resulting pellet, containing the pooled DRM fractions, was solubilized in Laemmli sample buffer (Laemmli 1970) and DRM proteins were separated by 12% reducing sodium dodecyl sulfate–polyacrylamide gel electrophoresis (SDS–PAGE) (Nour *et al.* 2004). The gel was stained with 0.25% Coomassie brilliant blue in 50% (v/v) methanol/10% (v/v) acetic acid for 30 min and destained with 25% (v/v) isopropanol/10% (v/v) acetic acid until the background was completely clear. The gel was subsequently dried using cellophane sheets (Bio-Rad Lab., Hercules, CA, USA) and scanned prior to selecting and excising bands for in-gel digestion. Eleven distinguishable Coomassie brilliant blue-stained bands (Fig. 1c) were excised from the gel and prepared from mass spectrometric analysis as described below.

In-gel digestion of protein bands was performed as described previously (Matsumoto and Komori 2000). Briefly, protein bands excised from gels were destained with 50% (v/v) acetonitrile/100 mmol/L ammonium bicarbonate (pH 8.9). In-gel digestion of each protein was performed with sequence-grade modified trypsin (Promega, Madison, WI, USA). Tryptic peptides were extracted from gels with 50% (v/v) acetonitrile/5% (v/v) trifluoroacetic acid, and concentrated using a Savant Speed-Vac concentrator. The tryptic peptides were dissolved in 0.2% trifluoroacetic acid, mixed with a matrix solution [10 mg/mL α-cyano-4-hydroxycinnamic acid in 50% (v/v) acetonitrile/0.1% (v/v) trifluoroacetic acid], and then applied to a target plate. Mass spectra were obtained using a matrix-assisted laser desorption/ionization time-of-flight (MALDI-TOF) mass spectrometer (Voyager Elite; PerSeptive Biosystems, Framingham, USA) and analyzed with the MASCOT peptide mass fingerprinting program (Matrix Science, London, UK; http://www.matrixscience.com). Database searches were performed against the National Center for Biotechnology Information (NCBI) non-redundant database using the following parameters: (i) the protein database under *Mammalia*; (ii) unlimited protein molecular weight and pI ranges; (iii) presence of protein modifications including acrylamide modification of cysteine, methionine oxidation, protein N-terminus acetylation, and pyroglutamic acid; and (iv) peptide mass tolerance of ±0.25 or 0.5 Da. MASCOT calculates the probability based MOWSE score that corresponds to the statistical significance of the peptide matching between an experimental protein and its candidate protein. In the current study, scores ≥69 correspond to $p < 0.05$. In order to confirm the identity of a protein candidate, MS/MS analysis of tryptic peptides was performed using a MALDI-quadrupole ion trap-TOF MS (Axima QIT; Shimadzu/Kratos, Manchester, UK). MS/MS data for each protein were analyzed using the MASCOT MS/MS ion search program (Matrix Science, London, UK). We considered the confirmation to be positive when the peptides that we analyzed for confirmation obtained, either individually or together, a significant MASCOT score (≥40, $p < 0.05$).

Lipid analyses of disk- and PM-derived DRMs

Disk- and PM-derived DRM fractions were collected and concentrated by centrifugation as described for the proteomic analyses. DRMs and the respective starting membranes (either disk or PM fractions) were subjected to a two-part extraction procedure to separate saponifiable from non-saponifiable lipids. Briefly, samples were supplemented with internal standards [19-hydroxycholesterol (Steraloids, Inc.; Newport, RI, USA) and 15: 0, 17: 0, and 21: 0 fatty acid standards (Nu-Chek Prep; Elysian, MN, USA)] prior to saponification with 2% (w/v) KOH at 100°C for 1 h. Distilled H_2O (0.5 mL) was added, the non-saponifiable lipids were extracted five times into hexane and the recovered organic phases were pooled. The aqueous phase was acidified by addition of 200 μL of concentrated HCl and sonicated for 10 min prior to extraction five times into hexane (this organic phase contains saponified fatty acids). Both saponifiable and non-saponifiable lipid extracts were dried under N_2 and the non-saponifiable lipids are resuspended in 50 μL of methanol for HPLC injection. Cholesterol was separated on a C18 column (Supelcosil LC-18; 25 cm × 4.6 mm; 5 μm particle size) with an isocratic mobile phase of 1 mL/min methanol. Detection was at 208 nm using an Agilent 1100 series photodiode array detector (Agilent Technologies, Inc., Santa Clara, CA, USA); cholesterol was quantified based upon absorbance at 208 nm, in comparison with an authentic cholesterol standard (within the linear response range), and corrected for recovery of the 19-hydroxycholesterol internal standard. The fatty acid extract was analyzed as described previously (Martin *et al.* 2005).

Western blot analysis

Western blot analyses were performed as previously described (Nour *et al.* 2004). For all western blots, proteins were initially separated by reducing SDS–PAGE on 10% gels. Blots were probed with various primary antibodies at the following dilutions: anti-rod opsin (1D4), 1: 2000; anti-ABCA4 (Rim 3F4), 1: 10; anti-bovine Rom-1 (1C6), 1: 1000; anti-GARP (Garp

4B1), 1: 250; anti-Cav-1, 1: 250; and anti-Glut-1, 1: 200 in 1–5% BSA in Tris-buffered saline containing 0.1% Tween 20. Immunoreactivity was detected using horseradish peroxidase-conjugated secondary antibodies (1: 5000) and chemiluminescent detection (SuperSignal® West Dura Extended Duration Substrate; Pierce), followed by densitometric analysis using a Kodak IS2000R Imaging Station. Care was taken to ensure that all signals were within the linear range of the camera (i.e., below pixel saturation threshold). For the semiquantitative analysis of rod opsin in DRMs derived from disk- and PM-enriched fractions, blots were probed with secondary antibodies (1: 15 000) conjugated to IRDye 800CW and imaged using a Li-Cor Odyssey Infrared Imaging system (Li-Cor Biosciences, Lincoln, NE, USA). To determine the relative distribution of each protein throughout the gradient, the sums of signal intensities for each protein in all lanes of the blot was determined yielding a 'total' signal for the entire gradient. From this, a value for percent of total was calculated for each fraction by dividing the signal in each lane by the total. When separated by reducing SDS–PAGE, rod opsin typically forms a 'ladder' pattern comprised of the monomer (M_r ~ 39 kDa) and higher molecular weight aggregates (dimers, trimers, etc.). To estimate the quantity of rod opsin in DRM fractions, each band of the ladder in each lane was detected using Kodak Image Station 4000R software and the density values were combined, yielding a composite rod opsin content for each lane. These values (individual bands or composite rod opsin density) were plotted using GraphPad Prism® 4.03. At least three independent samples were analyzed and the mean and standard deviations were determined and plotted.

Immunohistochemistry

Light microscopic immunohistochemistry was performed essentially as described in detail previously for mouse retinas (Tan *et al.* 2001), with some modifications. Here we used freshly harvested bovine eyes refrigerated immediately after slaughter and transported from the abattoir to the lab on ice within 2 h. After dissection, retinas were fixed either in buffered mixed aldehydes (freshly prepared 2% paraformaldehyde and 0.1% glutaraldehyde in 0.1 mol/L sodium phosphate, pH 7.4) or in phosphate-buffered 4% paraformaldehyde (overnight, 4°C). Following rinses with ice-chilled 50 mmol/L glycine in 0.1 mol/L sodium phosphate, pH 7.4 (once) and 0.1 mol/L sodium phosphate, pH 7.4 (three times), specimens of retina (with and without RPE-choroid attached) were obtained using a 7-mm trephine, and were then processed for LR White resin embedment and sectioned as described previously (cited above). Tissue sections (0.75 μm thickness, on glass microscope slides) were incubated for 1 h at 25°C in a humidified chamber with 'blocking buffer' (phosphate-buffered saline containing 1% (w/v) radioimmunoassay-grade BSA and 5% (by vol.) normal goat serum). Primary antibody (or non-immune control serum) was then applied at the desired dilution (e.g., 1: 100 (by vol.) for anti-Cav-1, 1: 20 for anti-Glut-1, in blocking buffer) and incubation was carried out for 36 h at 4°C. After rinsing briefly with phosphate-buffered saline, sections were treated for 2 h at 25°C with 1 nm colloidal gold-conjugated goat anti-rabbit IgG secondary antibody (AuroProbe® One GAR, Amersham, Arlington Heights, IL, USA; diluted 1: 50 (by vol.) with blocking buffer). Silver intensification was performed with an IntenSE® M Silver Enhancement Kit (Amersham), per the directions of the manufacturer. Sections were then rinsed with distilled water, lightly counterstained with 1% (w/v) toluidine blue in 1% (w/v) sodium borate, rinsed again with distilled water, air dried, and coverslipped using Permount® (Fisher Scientific, Hampton, NH, USA). Sections were viewed and photographed with an Olympus BH-2 photomicroscope (Olympus America, Inc., Center Valley, PA, USA) in the auto-expose mode, using a DPlanApo 20UV objective (0.70 NA) for bright-field exposures and a SPlanApo 60 (1.40 NA) oil immersion objective with an Olympus BH-2 DCA dark-field condenser for dark-field exposures. Images were captured with a Nikon DXM1200 digital camera (Nikon Instruments, Inc., Melville, NY, USA), stored on a PC hard drive, and annotated using Adobe PhotoShop®.

Statistical analyses

Multivariate analysis of variance (ANOVA) with post hoc Newman–Keuls tests was used to assess statistical differences between comparison groups, with significance limit set at $p < 0.05$. All groups contained at least three independent samples.

Results

Peptide mass fingerprinting analysis of DRM proteins

ROS-derived DRM fractions were isolated by as described in Materials and methods and equivalent volumes (35 μL) of each fraction were subjected to SDS–PAGE (Fig. 1a). The relative distribution of Cav-1 from three independent preparations was plotted as a percent of the total Cav-1 on the gradients (Fig. 1b) and we found ~85% of it in the low buoyant density fractions 1–4. DRM fractions 1–4 were pooled and subjected to mass spectrometric analysis as described (see Materials and methods). From this analysis, we identified several ROS proteins not previously reported in DRM fractions (see Table 1), including ABCA4 (also known as ABCR), CNGα-1, CNGβ-1, and Glut-1. A representative MALDI-TOF MS spectrum of tryptic peptides from the CNGα-1 subunit is shown in Fig. 2a. Rod opsin and PDE6 subunits, two proteins previously reported in ROS-derived DRMs (Seno *et al.* 2001;Nair *et al.* 2002;Senin *et al.* 2004;Martin *et al.* 2005) were also identified (Table 1). The detection of Na^+/K^+ ATPase α3 suggests minor cross-contamination from photoreceptor inner segment PM within the DRM fractions. However, in a previous study of similarly-prepared bovine ROS-derived DRMs (Elliott *et al.* 2003), this protein was not detectable in the ROS starting material by immunoblotting. Peptide mass fingerprinting also identified a subunit of the vacuolar proton ATPase in ROS-derived DRMs although this was not confirmed by MS/MS or immunoblot analysis. Candidate proteins of interest were further confirmed by MALDI-QIT-TOF MS (MS/MS) and/or western blot analyses.

Confirmation of DRM Protein Candidates by MS/MS

Candidate proteins initially identified by peptide mass fingerprinting were subsequently analyzed by MS/MS to confirm their identities (Table 1). As indicated, Glut-1, ABCA4, CNGα-1, and CNGβ-1 were all confirmed by significant MOWSE scores in MS/MS analyses of three different peptides. The presence of these proteins in bovine ROS DRMs was further confirmed by western blotting, as shown below. The presence of the CNGα-1 subunit in bovine ROS DRM was determined by MS/MS of tryptic peptides derived from the CNGα-1 subunit (Fig. 2), but was not investigated further by western analysis.

Semi-Quantitative Densitometric Analysis of DRM Proteins

Although informative, the mass spectrometric data do not provide an indication of the relative quantities of the identified proteins in DRMs. Also, because of the sensitivity of such analytical methods, some identified proteins could conceivably represent only a relatively minor component of DRMs. Therefore, we set out to determine the relative proportion of these proteins in ROS-derived DRM fractions by semi-quantitative densitometric analysis of western blots of equivalent fractions from at least three independent DRM preparations (see Materials and methods). The relative distribution of each protein was plotted as a percent of the total in all fractions and compared to the distribution of Cav-1 (Fig. 3). Although care was taken to ensure that all detected bands were within the linear range of the CCD camera, it should be noted that experiments using pure recombinant proteins indicate that the chemiluminescent enzymatic reaction is saturable with relatively small amounts of purified proteins (1–5 pmol; data not shown). As a result, the immunoblot signals from extremely abundant proteins (e.g., rod opsin) would be outside the linear range of the chemiluminescent enzymatic reaction. Therefore, for semi-quantitative analysis of rod opsin, we used an infrared imaging system that

affords a 16-fold wider dynamic range (Li-Cor Biosciences) than the conventional detection systems.

Mass spectrometric analyses indicated the presence of the integral disk membrane protein ABCA4, as well as rod opsin, which is abundant in disks, but is also present in ROS PM (Molday and Molday 1987). Although identified and confirmed by MS/MS, our immunoblot analysis indicated that only ~3% of total ABCA4 localized to DRM fractions (Fig. 3a) thus, it is unclear whether it is a bona fide DRM protein or a contaminant arising during DRM fractionation. As shown in Fig. 3b, the majority (~85%) of rod opsin was found in non-DRM fractions; however, ~15% of the total rod opsin (based upon densitometric analysis of western blots) was associated with DRM fractions, in agreement with previous reports (Seno *et al.* 2001; Elliott *et al.* 2003; Senin *et al.* 2004).

As shown in Fig. 3c, the majority of Glut-1 fractionated with the ROS-derived DRMs (>80% of total ROS-associated Glut-1). The DRM fractions isolated likely consist of a heterogeneous population of raft domains (Pike 2004); thus, co-fractionation of Glut-1 with Cav-1 does not necessarily indicate that the two proteins coexist within the same membrane domain. To determine whether Glut-1 and Cav-1 interact with one another, co-immunoprecipitation experiments were performed using monospecific antibodies against each protein; however, each antibody only effected immunoprecipitation of its cognate antigen (data not shown), suggesting a lack of interaction between Glut-1 and Cav-1.

Our analysis also demonstrated an enrichment of the CNGβ-1 subunit (~70 % of total) in DRM fractions (Fig. 3d). Unfortunately, because of species specificity issues with the CNGα-1 antibody, we were unable to determine the relative distribution of this subunit on DRM gradients. However, given that MS/MS data confirmed the presence of CNGα-1 in the DRM fractions, one might predict a distribution pattern similar to that observed for the CNG β-1 subunit (Fig. 3d).

Immunogold Labeling of Cav-1 and Glut-1 in Bovine Retina

Given the dramatic co-fractionation of Glut-1 and Cav-1 in DRMs we sought to assess their localizations in bovine retina tissue sections and to determine whether these proteins were present in the same cellular locations. The immunogold labeling pattern obtained with Cav-1 antibodies (gold-conjugated secondary, with silver enhancement) is shown in Fig. 4a. The photoreceptor inner segment (IS) layer was most prominently labeled, as were the endothelial cells that line the lumen of retinal blood vessels. The inner and outer plexiform layers also were more moderately immunopositive for Cav-1, whereas the outer and inner nuclear layers, ganglion cell layer, and photoreceptor OS layer were minimally and diffusely labeled. The localization of Cav-1 in the outer retina is similar to that observed in isolated bovine photoreceptors (Elliott *et al*. 2003). In contrast, the ONL and inner plexiform layer exhibited the most robust immunolabeling with anti-Glut-1 antibodies (Fig. 4b), with comparatively more moderate labeling of the outer plexiform layer, inner nuclear layer and ganglion cell layer, and only extremely sparse, diffuse labeling of the IS and OS layers. Thus, although both Cav-1 and Glut-1 co-localize to OS membranes, only a very minor fraction of the retina's total compliment of these proteins is localized to the OS layer. The lack of robust labeling of the ROS membranes with these two raft markers suggests that DRMs represent only a small fraction of the total ROS membrane surface area. This finding is consistent with the fact that ROS membranes are cholesterol-deficient, relative to typical PMs (Boesze-Battaglia and Albert 1992) and is also consistent with previous biochemical estimates that DRMs represent ~8% of the total ROS fatty acid (Martin *et al.* 2005). This finding is expanded upon in the current study where we provide lipid analytical data on DRMs derived from isolated ROS disk- and PM-enriched fractions.

Subfractionation and Analysis of ROS Disks and PM

Given the dramatic enrichment of two PM proteins to ROS-derived DRMs, we sought to examine the relative contributions and compositions of the distinct constituent membranes (disks vs. PM) of the ROS. Therefore, disk- and PM-enriched fractions were isolated by Ficoll flotation as described in Materials and methods. This 'modified Smith/Litman method' (Smith and Litman 1982) was chosen over an alternative, well-characterized disk/PM isolation procedure ['Molday method' (Molday and Molday 1987)] for reasons indicated below. The purity of our disk and PM fractions is indicated in Figs 5a and 8a. The modified Smith/Litman method is optimized for the isolation of osmotically intact disks, which float to the Ficoll-air interface upon ultracentrifugation; in contrast, following osmotic shock, the PM, the basal-most (so-called 'open') disks, and also the osmotically fragile disks tend to trap Ficoll upon resealing and subsequently pellet when subjected to ultracentrifugation. In turn, any PM adherent to osmotically-intact disks [e.g., via association between the CNGβ-1 GARP domain and Rds (Poetsch *et al.* 2001)] would be predicted to fractionate in the buoyant disk fraction. The detection of small amounts of Rds and the association of CNGβ-1 with the PM and disk fractions, respectively, is consistent with this. Although trypsin treatment has been shown to eliminate this association by removing the GARP portion of CNGβ-1 (Poetsch *et al.* 2001), we avoided this treatment because it potentially could affect partitioning of proteins to DRM domains. At least some of the membranes in our PM-enriched fraction may represent the basal-most population of ROS disks. However, the cross-contamination of these membranes is expected to be relatively low given: (i) the nearly quantitative fractionation of Glut-1 in PM-enriched fractions (Fig. 5a); (ii) the dramatic enrichment of Rds in disk-enriched fractions (Fig. 5a); and (iii) the marked and predictable differences in cholesterol (Fig. 7a) and fatty composition (Fig. 8a). In fact, the results of our cholesterol and fatty acid analyses of disk-and PM-enriched fractions are quite similar to those reported previously (Boesze-Battaglia and Albert 1989, 1990) using highly purified ROS disks and PM prepared by the Molday method.

While both disks and PM share some protein components (e.g., rod opsin), they also have distinct proteins unique to each fraction. As previously observed (Smith and Litman 1982), a protein having the apparent relative molecular weight (M_r) of rod opsin accounts for ~90% of the total stained protein in our disk-enriched fraction (Fig. 5a, upper panel). CNGβ-1 and Rds exhibited preferential enrichment in ROS disks, compared to PM, while Glut-1 showed an absolute preference for PM, compared to disks (Fig. 5a (lower panel). Cav-1 was present both in PM and disks, but exhibited a 2.8-fold enrichment in the PM fraction based on densitometric analysis of 4 independent preparations.

Having obtained PM- and disk membrane-enriched fractions, we then proceeded to subfractionate each to obtain DRM and non-DRM fractions (Fig. 5b and c). Very little rod opsin was detectable in PM-derived DRMs (Fig. 5b; see also semi-quantitative analysis, Fig. 6). However, Glut-1 exhibited marked enrichment in these fractions; hence, the overwhelming majority of Glut-1 found in ROS PM is DRM-associated. Note that, in both cases, the distribution of protein is approximately equal in fractions 4 and 5. In contrast, while only about 30% of the total CNGβ-1 coincides with these DRM fractions, the distribution within these fractions is decidedly unequal, with about 80% of the CNG β-1 preferentially located in fraction 5 (see Discussion). Companion analysis of disk membrane fractions (Fig. 5c) revealed substantially different results than that obtained with the PM-enriched fraction. For one, there was a notable shift to lighter densities for the Cav-1-containing fractions, compared to that of PM (cf. Fig. 5b), with the majority being distributed approximately equally between fractions 3 and 4. Secondly, at least half of the total CNGβ-1 in disks was distributed in DRM fractions, with the majority of that being localized to fractions 3 and 4 (not fraction 5, as found for PM). Again, we believe that the presence of CNG channel in these disk preparations is artifactual (see Discussion above), and does not represent its true localization *in vivo.* In contrast to the

PM-enriched fractions, there was a significant pool of rod opsin detectable in DRM fractions 4 and 5 derived from disk-enriched membranes (Fig. 5c). The semi-quantitative analyses of rod opsin distribution from three independent disk- and PM-enriched DRM preparations are presented in Fig. 6a (representative blots different from those presented in Fig. 5 are shown in Fig. 6b and c). Notably, only ~2% of the total rod opsin fractionates to DRMs (fractions 2–4) derived from PM-enriched membranes whereas ~16% of the total rod opsin is found in DRM fractions 2–4 isolated from disk membranes. The results observed for disk membranes are similar to those observed for ROS membranes in general [Fig. 3b; and (Seno *et al.* 2001; Senin *et al.* 2004)]. Notably, there was no detectable Glut-1 in any disk fraction (data not shown). While the majority of Rom-1 in disks was distributed in the higher density sucrose gradient zone (fractions 7 and 8), an appreciable percentage was found in the DRM fractions (Fig. 5c). The distribution of Rds was qualitatively similar (data not shown) consistent with the results shown for the representative starting materials (Fig. 5a). In sum, these results highlight the heterogeneity of the DRM populations in ROS PM vs. disk membranes, which may indicate distinct compositional differences between raft domains.

Lipid analyses of DRM fractions from disks and PM

Next, we assessed the relative concentration of cholesterol in disks vs. PM, and DRM-enriched fractions derived there from. The results, normalizing cholesterol (chol) content to total phospholipid (PL) content on a mole basis, are shown in Fig. 7a. As expected, there was an enrichment of cholesterol in DRM fractions, compared to the initial membranes from which they were derived, both in ROS disks and PM. Normalizing cholesterol content to total protein showed a similar trend (data not shown). For disks, comparing mean values, this enrichment was about twofold, while for PM it was about 1.5-fold. Notably, the mean chol/PL mole ratio of PM was about threefold greater than that of disks and about twofold greater than that of disk DRMs. Also, the mean chol/PL ratio of ROS PM-derived DRM was almost fourfold greater than that of disk-derived DRMs. Hence, there is a trend in the relative enrichment of cholesterol in these membranes: PM DRMs $\gg$ PM > disk DRMs > disks.

To further examine compositional differences between disks, PM, and DRMs derived there from, we determined the relative distribution of saturated, monounsaturated, and polyunsaturated fatty acid (PUFA) classes within and between these same membrane fractions. As shown in Fig. 7b, each of these membrane fractions exhibited its own signature pattern of fatty acid composition. For ROS disks, saturates and PUFA dominated (ca. 95% of total fatty acids) and were approximately equal in amount, whereas monounsaturates represented only about 5% of the total. In contrast, disk-derived DRM were enriched in saturated fatty acids (ca. 65% of total), being at least twofold higher than the amount of PUFA; again, monounsaturates represented a minor fraction (ca. 4%). For unfractionated ROS PM, while the relative ratio of saturated fatty acids to PUFA was approximately 2 (as for disk DRM), the relative amount of monounsaturates was substantially increased (ca. 17.5% of total), being ca. threefold higher than that of disks or disk DRM. The PM-derived DRM fraction exhibited yet another pattern: saturated fatty acids (ca. 67% of total) were approximately fourfold more prevalent than either monounsaturates or PUFA, the latter representing approximately equal percentages (ca. 16–17%) of the total fatty acids in this fraction. If we compare the saturated: PUFA mole ratios, the trend is as follows (ratio values given in parentheses): disks (0.98) < PM (2.04) < disk DRMs (2.31) $\ll$ PM DRMs (4.38). These trends in saturated/unsaturated fatty acids are generally consistent with the trends in the relative enrichment of cholesterol among these four membrane fractions: DRMs represent a cholesterol-enriched fraction, relative to non-DRM domains (Brown and London 2000;Simons and Vaz 2004), and cholesterol has a higher affinity for (packs more tightly with) saturated vs. unsaturated fatty acids (Xu and London 2000).

Having demonstrated dramatic variations in the fatty acid composition of ROS PM vs. disks and their constituent DRM fractions, we then examined the detailed fatty acid composition of each of these membrane preparations. The results are shown in Fig. 8. Overall, the fatty acid composition of these membrane fractions is relatively simple, with only 3–4 dominant species each representing at least 10 mol% of the total. In ROS disks (Fig. 8a), DHA (22: 6n3) represents nearly 30 mol% of the total fatty acids, being only slightly more prevalent than stearic acid (18: 0, ca. 27.5 mol%); palmitate (16: 0, ca. 20 mol%) is the third most prevalent fatty acid. Together, these three comprise ~80% of the total fatty acids in disk membranes; by comparison, oleate (18: 1), arachidonate (20: 4n6), and docosapentaenoate (22: 5n6) are relatively minor species, each accounting for only ca. 4–6 mol% of the total fatty acids. Comparing ROS disks vs. PM (Fig. 8a), DHA levels are nearly threefold higher in disks than in PM, where the dominant fatty acid species are 16: 0 and 18: 0 (each ca. 27–28 mol%), percentage-wise, 18: 1 is a significant species (>15 mol%) in PM, being nearly threefold more prevalent than in disk membranes. These findings are in general agreement with those previously reported by Boesze-Battaglia and Albert (Boesze-Battaglia and Albert 1989) and provide a further indication of the purity of the disk and PM-enriched starting materials. Comparing disks vs. their constituent DRM (Fig. 8b), these general trends tend to hold qualitatively; however, 16: 0 and 18: 0 are each ca. 31–32 mol% of total fatty acids in disk DRM, with 16: 0 being ca. 1.6-fold higher and DHA being ca. 1.9-fold lower in disk DRM, relative to unfractionated disks. The levels of 18: 1, 20: 4n6, and 22: 5n6 are comparable in disks and disk DRM (unlike the case for disks vs. PM, there is no difference in 18: 1 levels when comparing disks vs. disk DRM). Comparing ROS PM vs. DRM derived therefrom, while the DHA levels are low in PM compared to disks (see Fig. 8a), they were about twofold higher than in the PM-derived DRM fraction, where 16: 0 is the dominant fatty acid (nearly 40 mol %, ca. 1.4–fold higher than in PM). The levels of 18: 0 (ca. 26 mol%) and 18: 1 (ca. 14–15 mol %) are comparable in PM vs. PM-derived DRMs. Finally, comparing disk- vs. PM-derived DRM fractions, DHA levels are nearly threefold higher in disk DRMs. Also, while 16: 0 and 18: 0 are the dominant acyl species in both membrane fractions, accounting for ca. 65% of the total fatty acids, the levels of these species are nearly equivalent in disk DRMs, whereas in PM DRM there is ca. 1.5-fold more 16: 0 than 18: 0. In addition, 18: 1 levels are >2-fold higher in PM DRM than in disk DRM. In total, the data shown in Fig. 8 are very consistent with the composite fatty acid class data shown in Fig. 7b.

Discussion

A goal of the current study was to provide an analysis of the protein and lipid composition of ROS-derived DRMs to provide a biochemical framework to facilitate further studies on membrane microdomains in photoreceptors. Mass spectrometric analyses identified several novel proteins in DRM fractions (e.g., CNG channel subunits, and Glut-1) and subsequent immunoblot analyses demonstrated that the CNG channel β-subunit and Glut-1, both integral PM membrane proteins (Cook *et al.* 1989; Hsu and Molday 1991) are enriched in DRMs (Fig. 3).

The functional significance of the enrichment of the CNG channel in DRMs remains to be elucidated. Studies have shown a significant pool (~25%) of the homologous olfactory CNG channel (CNGA2) is localized to cholesterol-rich DRM and depletion of cholesterol by treatment with methyl-β-cyclodextrin effectively disrupted prostaglan-din-induced Ca^{2+} conductance (Brady *et al.* 2004). Membrane lipid composition may also regulate the activity of Glut-1 (Carruthers and Melchior 1984) and cholesterol depletion resulting in raft disruption causes increased Glut-1 transport activity (Barnes *et al.* 2004). Treatment of cells with azide, an inhibitor of oxidative phosphorylation, results in increased Glut-1 activity that correlates with a change in localization of Glut-1 from DRMs to non-DRM fractions (Rubin and Ismail-Beigi 2003). It is tempting to speculate that the lipid composition of membrane microdomains

in the ROS PM might regulate photoreceptor CNG channel and glucose transport activities in an analogous manner.

With well-characterized disk- and PM-enriched fractions in hand, we were able to address several outstanding issues regarding the contribution of each of these ROS membrane compartments to ROS-derived DRMs, including the contribution of PM to DRM rod opsin content. A portion (ca. 15%, based on immunoblot data) of the total rod opsin content of intact ROS membranes localized to DRMs [Fig. 3b, and (Seno *et al.* 2001;Senin *et al.* 2004)]. However, it was unclear whether rod opsin in DRMs isolated from intact ROS was derived predominantly from disks or PM. The current results demonstrate that rod opsin is relatively absent (only ~ 2% of the total) from PM-derived DRMs (Fig. 6), while ~16% of the total of disk-derived rod opsin fractionates to DRMs. In addition to the fact that the PM only represents <3% of total ROS membranes, these findings clearly demonstrate that the vast majority of rod opsin in ROS-derived DRM preparations originates from disks and provides further support to the idea that disk membranes contain raft-like domains.

Our results clearly demonstrate that DRMs can be isolated from disks. However, the localization of ABCA4 (ABCR), a resident protein of disk rims, deserves further discussion. Based on the presence of ROM-1, the rim region has been suggested to be a site of membrane heterogeneity in disks (Boesze-Battaglia *et al.* 2002). Although detected and identified in our mass spectrometric analyses disk-derived DRMs (Table 1), ABCA4 was not an abundant protein component of such membrane domains (Fig. 3a), suggesting that ROM-1 and ABCA4 reside in biophysically-distinct membrane domains. The transported ligand of ABCA4 has been identified as the protonated Schiff's base complex of all-*trans* retinaldehyde and phosphatidylethanolamine (*N*-retinylidene-PE) (Sun *et al.* 1999; Weng *et al.* 1999; Ahn *et al.* 2000; Sun and Nathans 2001; Beharry *et al.* 2004). We have previously reported that phosphatidylethanolamine is relatively enriched in non-DRM fractions derived from intact ROS membranes (Martin *et al.* 2005). Thus, although speculative, it is perhaps not surprising that ABCA4 preferentially fractionates to non-DRM (i.e., phosphatidylethanolamine-deficient) membrane domains. It is presently unknown whether N-retinylidene-PE is enriched in DRMs, but this could be pursued further by comparative analysis of microdomain composition in ABCA4-null vs. wild-type mice.

Additional features regarding compositional differences between disk and PM-derived DRMs became evident when the fractionation of proteins to these domains was analyzed (Figs 5b, c and 6). While PM and disks were found to contain DRMs, as evidenced by the presence of low buoyant density fractions containing Cav-1, the relative distribution of Cav-1 in these fractions was not identical: the majority of Cav-1 in disk DRMs was found in fractions 3 and 4 (somewhat more in 3 than in 4), while in PM-derived DRMs the majority of Cav-1 was found distributed approximately equally in fractions 4 and 5. This may indicate differences in the lipid/protein ratios of DRMs from disks vs. PM. The heterogeneity of DRM populations is further indicated by the differential distribution of certain marker proteins and also by differences in lipid composition, including chol: PL mole ratios (Fig. 7a), fatty acid class composition (saturated/unsaturated ratios; Fig. 7b), and detailed fatty acid species differences (Fig. 8). The cholesterol content of disks is heterogeneous with the highest content present in newly synthesized disks (Boesze-Battaglia *et al.* 1990), which are located basally (proximal to the connecting cilium of the photoreceptor), and these results correlate with the observed distribution of PFPs on disks (Andrews and Cohen 1979). Given the relative paucity of cholesterol in apical disks (proximal to the retinal pigment epithelium), relative to the more basally located disks, it is most likely that disk-derived DRMs are derived largely from basal, rather than apical, disks.

From these detailed composition analyses, it now is clear that DRMs in ROS disks are distinct from those in ROS PM. Furthermore, lipid analyses demonstrated that PM-derived DRMs have

nearly a threefold higher cholesterol content and a ca. 1.6-fold higher saturated/PUFA ratio than disk DRMs. In addition, the DHA content of disk DRMs is about twofold greater than in PM DRMs. The markedly different lipid environment of DRMs in disks vs. PM would be predicted to significantly impact the biophysical and functional properties of membrane proteins in these domains. Given the considerably greater enrichment of cholesterol and higher saturated/PUFA ratio in PM compared to disks, we initially predicted that DRMs would represent a proportionately larger percentage of the total membrane mass in PM than in disks; however, this turns out not to be the case. Based upon the results of our fatty acid analyses, DRMs represent ~8% of the disk membrane and ~12% of the PM. We recovered 13% and 18% of the total cholesterol in the disk and PM-derived DRM fractions, respectively, suggesting that the majority of cholesterol is present in the bulk phase; alternatively, Triton X-100 solubilization may have disrupted a portion of the DRMs (Schuck *et al.* 2003). However, the enrichment of Cav-1 in DRMs suggests, at least, that our treatment did not solubilize Cav-1-enriched microdomains.

The results of this study suggest that membrane microdomains may be relatively abundant in ROS PM, consistent with previous observations on cholesterol distribution in ROS membranes and the abundance of PFPs. The ROS PM has a cholesterol/phospholipid mole ratio of ~0.40 (Boesze-Battaglia and Albert 1989), compared to disk membranes, which average ~0.12 (Fliesler and Anderson 1983; Boesze-Battaglia *et al.* 1989); our present results are consistent with these prior findings. Previous studies have shown a sixfold gradient in the cholesterol content of ROS disks, with basal disks exhibiting a cholesterol/phospholipid ratio of ~0.30 and the most apical disks having a ratio of ~0.05 (Boesze-Battaglia *et al.* 1990). Given the requirement of cholesterol to form lipid raft microdomains (Brown and London 2000; Pike 2004), these findings correlate well with the distribution of cholesterol-rich, PFPs observed by freeze-fracture electron microscopy, because such patches were prominent in PM and basal, but not apical, disks (Andrews and Cohen 1979). However, it is surprising that a relatively similar proportion of disk membranes also contain DRMs and that the majority of DRM-associated rod opsin is disk-derived, even though the majority of disks are relatively cholesterol-deficient. The exact correlation between DRMs (a persistent, biochemically isolated membrane fraction) and *bona fide* lipid rafts (dynamic and transient membrane domains existing *in vivo*) remains a matter of considerable controversy (Shogomori and Brown 2003; Silvius 2005; Brown 2006; Hancock 2006; Shaw 2006; Jacobson *et al.* 2007). While it is tempting to speculate that PFPs, DRMs, and lipid rafts share the same identity, more definitive proof is necessary to make this claim compelling. However, the current study provides a biochemical framework to facilitate further studies on membrane microdomains in photoreceptors.

Prior studies have shown that cholesterol can bind to rod opsin (Albert *et al.* 1996b) and that a high-cholesterol membrane environment suppresses the transductional competence of rod opsin by decreasing its ability to become activated [(Boesze-Battaglia and Albert 1990; Albert *et al.* 1996a; Niu *et al.* 2001, 2002); reviewed in (Albert and Boesze-Battaglia 2005)]. These facts are inconsistent with DRMs serving the function of platforms that support phototransduction in the ROS. Instead, DRMs may represent reservoirs that dynamically and transiently sequester phototransduction cascade components in a transductionally silent state; upon release from the high-cholesterol DRM environment, these components may then re-engage in phototransduction. Based upon the results presented herein, a hypothetical model of membrane domain organization in photoreceptor disk and PM is presented in Fig. 9 and expands upon the model presented by Boesze-Battaglia *et al.* (2002). Our model summarizes the findings that the majority of disk-derived rod opsin is located in the bulk (non-DRM) phase, with only a modest portion found in DRMs; in contrast, essentially all rod opsin in the PM is found in the bulk phase. In addition, most of the CNG ion channel and essentially all Glut-1 transporter from the ROS PM are DRM-associated. Rom-1, Rds, and ABCA4 are exclusively

localized to the ROS disks; within the disks, most of the Rom-1 and essentially all of the Rds and ABCA4 are found in non-DRM domains. For simplicity, peripherally-associated proteins that have been previously reported in DRMs (e.g., transducin, cGMP-PDE, and guanylate cyclase) are not shown.

In conclusion, the current study provides a host of new information regarding membrane domains in ROS. Here, we provide the first mass spectrometric analyses of ROS-derived DRMs and identify several novel DRM-associated proteins including the CNG channel and the Glut-1 transporter. This clearly indicates that both ROS plasma and disk membranes contain DRM domains. We also provide the first detailed fatty acid analysis of DRM domains isolated from ROS disks and PM. We show that DRMs represent approximately 8% of disks and 12% of ROS PM, and that the lipid environment of disk DRMs is markedly distinct from that of PM-derived DRMs. In addition, we demonstrate that the majority of rod opsin observed in DRMs is, rather surprisingly, derived from disks. Although the integral disk protein, ABCA4, is present in ROS-derived DRMs (based on sensitive mass spectrometric analyses), it is relatively less abundant than either of two integral PM proteins, CNGβ-1 or Glut-1, both of which are enriched in DRMs, relative to non-DRM domains. The exact relationship between these biochemically-isolated DRM fractions and the *bona fide* raft domains in native ROS membranes *in vivo* is currently under investigation.

Acknowledgments

We thank Dr. Muayyad Al-Ubaidi for critical evaluation of the manuscript, Barbara A. Nagel for technical help on the immuno-histochemistry, and R. Steven Brush for assistance with statistical analyses. We also thank Dr. Robert S. Molday for generously supplying some of the antibodies used in this study. This study was supported by grants from the National Institutes of Health [EY10609 (MIN), EY016201 (MIN), EY13877 (HM), EY007361 (SJF), RR017703 from the COBRE Program of the National Center for Research Resources (MHE), and a Core Grant for Vision Research EY012190 (MIN, MHE)], by the Foundation Fighting Blindness (MIN), by the Norman J. Stupp Foundation Charitable Trust (SJF), and by unrestricted departmental grants from Research to Prevent Blindness (MHE and SJF). The content is solely the responsibility of the authors and does not necessarily represent the official views of the National Center For Research Resources, the National Eye Institute, or the National Institutes of Health. SJF is the recipient of a Research to Prevent Blindness Senior Scientific Investigator Award.

Abbreviations

ABCA4	ATP-binding cassette transporter superfamily class A number 4
BSA	bovine serum albumin
Cav-1	caveolin-1
chol	cholesterol
CNGβ-1	cyclic nucleotide-gated channel beta-1 subunit
DHA	docosahexaenoic acid
DRM	detergent-resistant membrane
GARP	glutamic acid-rich protein
Glut-1	glucose transporter type 1
IS	inner segment
MALDI-TOF	matrix-assisted laser desorption/ionization time-of-flight
PDE6	cGMP-phosphodiesterase
PFPs	particle-free patches
PL	phospholipid

PM	plasma membrane
PUFA	polyunsaturated fatty acid
Rds	retinal degeneration slow protein
Rom-1	rod outer segment membrane protein 1
ROS	rod outer segment
Tα	transducin alpha subunit
Tβγ	transducin beta-gamma subunits

References

Ahn J, Wong JT, Molday RS. The effect of lipid environment and retinoids on the ATPase activity of ABCR, the photoreceptor ABC transporter responsible for Stargardt macular dystrophy. J Biol Chem 2000;275:20399–20405. [PubMed: 10767284]

Albert AD, Boesze-Battaglia K. The role of cholesterol in rod outer segment membranes. Prog Lipid Res 2005;44:99–124. [PubMed: 15924998]

Albert AD, Boesze-Battaglia K, Paw Z, Watts A, Epand RM. Effect of cholesterol on rhodopsin stability in disk membranes. Biochim Biophys Acta 1996a;1297:77–82. [PubMed: 8841383]

Albert AD, Young JE, Yeagle PL. Rhodopsin-cholesterol interactions in bovine rod outer segment disk membranes. Biochim Biophys Acta 1996b;1285:47–55. [PubMed: 8948474]

Allen JA, Halverson-Tamboli RA, Rasenick MM. Lipid raft microdomains and neurotransmitter signalling. Nat Rev Neurosci 2007;8:128–140. [PubMed: 17195035]

Andrews LD, Cohen AI. Freeze-fracture evidence for the presence of cholesterol in particle-free patches of basal disks and the plasma membrane of retinal rod outer segments of mice and frogs. J Cell Biol 1979;81:215–228. [PubMed: 314450]

Arshavsky VY, Lamb TD, Pugh EN Jr. G proteins and phototransduction. Annu Rev Physiol 2002;64:153–187. [PubMed: 11826267]

Barnes K, Ingram JC, Bennett MD, Stewart GW, Baldwin SA. Methyl-beta-cyclodextrin stimulates glucose uptake in Clone 9 cells: a possible role for lipid rafts. Biochem J 2004;378:343–351. [PubMed: 14616090]

Beharry S, Zhong M, Molday RS. N-retinylidene-phosphatidylethanolamine is the preferred retinoid substrate for the photoreceptor-specific ABC transporter ABCA4 (ABCR). J Biol Chem 2004;279:53972–53979. [PubMed: 15471866]

Boesze-Battaglia K, Albert AD. Fatty acid composition of bovine rod outer segment plasma membrane. Exp Eye Res 1989;49:699–701. [PubMed: 2806432]

Boesze-Battaglia K, Albert AD. Cholesterol modulation of photoreceptor function in bovine retinal rod outer segments. J Biol Chem 1990;265:20727–20730. [PubMed: 2174424]

Boesze-Battaglia K, Albert AD. Phospholipid distribution among bovine rod outer segment plasma membrane and disk membranes. Exp Eye Res 1992;54:821–823. [PubMed: 1623969]

Boesze-Battaglia K, Hennessey T, Albert AD. Cholesterol heterogeneity in bovine rod outer segment disk membranes. J Biol Chem 1989;264:8151–8155. [PubMed: 2722776]

Boesze-Battaglia K, Fliesler SJ, Albert AD. Relationship of cholesterol content to spatial distribution and age of disc membranes in retinal rod outer segments. J Biol Chem 1990;265:18867–18870. [PubMed: 2229047]

Boesze-Battaglia K, Dispoto J, Kahoe MA. Association of a photoreceptor-specific tetraspanin protein, ROM-1, with triton X-100-resistant membrane rafts from rod outer segment disk membranes. J Biol Chem 2002;277:41843–41849. [PubMed: 12196538]

Brady JD, Rich TC, Le X, Stafford K, Fowler CJ, Lynch L, Karpen JW, Brown RL, Martens JR. Functional role of lipid raft microdomains in cyclic nucleotide-gated channel activation. Mol Pharmacol 2004;65:503–511. [PubMed: 14978228]

Brown DA. Lipid rafts, detergent-resistant membranes, and raft targeting signals. Physiology (Bethesda) 2006;21:430–439. [PubMed: 17119156]

Brown DA, London E. Structure and function of sphingolipid- and cholesterol-rich membrane rafts. J Biol Chem 2000;275:17221–17224. [PubMed: 10770957]

Brown DA, Rose JK. Sorting of GPI-anchored proteins to glycolipid-enriched membrane subdomains during transport to the apical cell surface. Cell 1992;68:533–544. [PubMed: 1531449]

Carruthers A, Melchior DL. Human erythrocyte hexose transporter activity is governed by bilayer lipid composition in reconstituted vesicles. Biochemistry 1984;23:6901–6911. [PubMed: 6543323]

Chen CK. The vertebrate phototransduction cascade: amplification and termination mechanisms. Rev Physiol Biochem Pharmacol 2005;154:101–121. [PubMed: 16634148]

Cook NJ, Molday LL, Reid D, Kaupp UB, Molday RS. The cGMP-gated channel of bovine rod photoreceptors is localized exclusively in the plasma membrane. J Biol Chem 1989;264:6996–6999. [PubMed: 2468664]

Elliott MH, Fliesler SJ, Ghalayini AJ. Cholesterol-dependent association of caveolin-1 with the transducin alpha subunit in bovine photoreceptor rod outer segments: disruption by cyclodextrin and guanosine 5′-O-(3-thiotriphosphate). Biochemistry 2003;42:7892–7903. [PubMed: 12834341]

Fliesler SJ, Anderson RE. Chemistry and metabolism of lipids in the vertebrate retina. Prog Lipid Res 1983;22:79–131. [PubMed: 6348799]

Foster LJ, de Hoog CL, Mann M. Unbiased quantitative proteomics of lipid rafts reveals high specificity for signaling factors. Proc Natl Acad Sci USA 2003;100:5813–5818. [PubMed: 12724530]

Fotiadis D, Liang Y, Filipek S, Saperstein DA, Engel A, Palczewski K. The G protein-coupled receptor rhodopsin in the native membrane. FEBS Lett 2004;564:281–288. [PubMed: 15111110]

Gupta N, Wollscheid B, Watts JD, Scheer B, Aebersold R, DeFranco AL. Quantitative proteomic analysis of B cell lipid rafts reveals that ezrin regulates antigen receptor-mediated lipid raft dynamics. Nat Immunol 2006;7:625–633. [PubMed: 16648854]

Hancock JF. Lipid rafts: contentious only from simplistic standpoints. Nat Rev Mol Cell Biol 2006;7:456–462. [PubMed: 16625153]

Hsu SC, Molday RS. Glycolytic enzymes and a GLUT-1 glucose transporter in the outer segments of rod and cone photoreceptor cells. J Biol Chem 1991;266:21745–21752. [PubMed: 1939198]

Isshiki M, Anderson RG. Function of caveolae in $Ca2^{+}$ entry and $Ca2^{+}$ -dependent signal transduction. Traffic 2003;4:717–723. [PubMed: 14617355]

Jacobson K, Mouritsen OG, Anderson RG. Lipid rafts: at a crossroad between cell biology and physics. Nat Cell Biol 2007;9:7–14. [PubMed: 17199125]

Kaminski WE, Piehler A, Wenzel JJ. ABC A-subfamily transporters: structure, function and disease. Biochim Biophys Acta 2006;1762:510–524. [PubMed: 16540294]

Keller RK, Arnold TP, Fliesler SJ. Formation of 7-dehydrocholesterol-containing membrane rafts in vitro and in vivo, with relevance to the Smith-Lemli-Opitz syndrome. J Lipid Res 2004;45:347–355. [PubMed: 14594996]

Kusumi A, Suzuki K. Toward understanding the dynamics of membrane-raft-based molecular interactions. Biochim Biophys Acta 2005;1746:234–251. [PubMed: 16368465]

Laemmli UK. Cleavage of structural proteins during the assembly of the head of bacteriophage T4. Nature 1970;227:680–685. [PubMed: 5432063]

Laude AJ, Prior IA. Plasma membrane microdomains: organization, function and trafficking. Mol Membr Biol 2004;21:193–205. [PubMed: 15204627]

Le Naour F, Andre M, Boucheix C, Rubinstein E. Membrane microdomains and proteomics: lessons from tetraspanin microdomains and comparison with lipid rafts. Proteomics 2006;6:6447–6454. [PubMed: 17109380]

Li N, Shaw AR, Zhang N, Mak A, Li L. Lipid raft proteomics: analysis of in-solution digest of sodium dodecyl sulfate-solubilized lipid raft proteins by liquid chromatography-matrix-assisted laser desorption/ionization tandem mass spectrometry. Proteomics 2004;4:3156–3166. [PubMed: 15378691]

Liang Y, Fotiadis D, Filipek S, Saperstein DA, Palczewski K, Engel A. Organization of the G protein-coupled receptors rhodopsin and opsin in native membranes. J Biol Chem 2003;278:21655–21662. [PubMed: 12663652]

Liu H, Seno K, Hayashi F. Active transducin alpha subunit carries PDE6 to detergent-resistant membranes in rod photoreceptor outer segments. Biochem Biophys Res Commun 2003;303:19–23. [PubMed: 12646160]

Martin RE, Elliott MH, Brush RS, Anderson RE. Detailed characterization of the lipid composition of detergent-resistant membranes from photoreceptor rod outer segment membranes. Invest Ophthalmol Vis Sci 2005;46:1147–1154. [PubMed: 15790872]

Matsumoto H, Komori N. Ocular proteomics: cataloging photoreceptor proteins by two-dimensional gel electrophoresis and mass spectrometry. Methods Enzymol 2000;316:492–511. [PubMed: 10800697]

Maw MA, Corbeil D, Koch J, et al. A frameshift mutation in prominin (mouse)-like 1 causes human retinal degeneration. Hum Mol Genet 2000;9:27–34. [PubMed: 10587575]

Molday RS. Photoreceptor membrane proteins, phototransduction, and retinal degenerative diseases. The Friedenwald Lecture. Invest Ophthalmol Vis Sci 1998;39:2491–2513. [PubMed: 9856758]

Molday RS, Molday LL. Differences in the protein composition of bovine retinal rod outer segment disk and plasma membranes isolated by a ricin-gold-dextran density perturbation method. J Cell Biol 1987;105:2589–2601. [PubMed: 2447095]

Nair KS, Balasubramanian N, Slepak VZ. Signal-dependent translocation of transducin, RGS9-1-Gbeta5L complex, and arrestin to detergent-resistant membrane rafts in photoreceptors. Curr Biol 2002;12:421–425. [PubMed: 11882295]

Nair KS, Hanson SM, Kennedy MJ, Hurley JB, Gurevich VV, Slepak VZ. Direct binding of visual arrestin to microtubules determines the differential subcellular localization of its splice variants in rod photoreceptors. J Biol Chem 2004;279:41240–41248. [PubMed: 15272005]

Niu SL, Mitchell DC, Litman BJ. Optimization of receptor-G protein coupling by bilayer lipid composition II: formation of metarhodopsin II-transducin complex. J Biol Chem 2001;276:42807–42811. [PubMed: 11544259]

Niu SL, Mitchell DC, Litman BJ. Manipulation of cholesterol levels in rod disk membranes by methyl-beta-cyclodextrin: effects on receptor activation. J Biol Chem 2002;277:20139–20145. [PubMed: 11889130]

Nour M, Ding XQ, Stricker H, Fliesler SJ, Naash MI. Modulating expression of peripherin/rds in transgenic mice: critical levels and the effect of overexpression. Invest Ophthalmol Vis Sci 2004;45:2514–2521. [PubMed: 15277471]

Pike LJ. Lipid rafts: bringing order to chaos. J Lipid Res 2003;44:655–667. [PubMed: 12562849]

Pike LJ. Lipid rafts: heterogeneity on the high seas. Biochem J 2004;378:281–292. [PubMed: 14662007]

Pike LJ. Rafts defined: a report on the Keystone Symposium on Lipid Rafts and Cell Function. J Lipid Res 2006;47:1597–1598. [PubMed: 16645198]

Pike LJ, Han X, Chung KN, Gross RW. Lipid rafts are enriched in arachidonic acid and plasmenylethanolamine and their composition is independent of caveolin-1 expression: a quantitative electrospray ionization/mass spectrometric analysis. Biochemistry 2002;41:2075–2088. [PubMed: 11827555]

Poetsch A, Molday LL, Molday RS. The cGMP-gated channel and related glutamic acid-rich proteins interact with peripherin-2 at the rim region of rod photoreceptor disc membranes. J Biol Chem 2001;276:48009–48016. [PubMed: 11641407]

Resh MD. Fatty acylation of proteins: new insights into membrane targeting of myristoylated and palmitoylated proteins. Biochim Biophys Acta 1999;1451:1–16. [PubMed: 10446384]

Ridge KD, Abdulaev NG, Sousa M, Palczewski K. Phototransduction: crystal clear. Trends Biochem Sci 2003;28:479–487. [PubMed: 13678959]

Roper K, Corbeil D, Huttner WB. Retention of prominin in microvilli reveals distinct cholesterol-based lipid micro-domains in the apical plasma membrane. Nat Cell Biol 2000;2:582–592. [PubMed: 10980698]

Rubin D, Ismail-Beigi F. Distribution of Glut1 in detergent-resistant membranes (DRMs) and non-DRM domains: effect of treatment with azide. Am J Physiol Cell Physiol 2003;285:C377–C383. [PubMed: 12686514]

Schuck S, Honsho M, Ekroos K, Shevchenko A, Simons K. Resistance of cell membranes to different detergents. Proc Natl Acad Sci USA 2003;100:5795–5800. [PubMed: 12721375]

Senin II, Hoppner-Heitmann D, Polkovnikova OO, Churumova VA, Tikhomirova NK, Philippov PP, Koch KW. Recoverin and rhodopsin kinase activity in detergent-resistant membrane rafts from rod outer segments. J Biol Chem 2004;279:48647–48653. [PubMed: 15355976]

Seno K, Kishimoto M, Abe M, Higuchi Y, Mieda M, Owada Y, Yoshiyama W, Liu H, Hayashi F. Light- and guanosine 5′-3-O-(thio)triphosphate-sensitive localization of a G protein and its effector on detergent-resistant membrane rafts in rod photoreceptor outer segments. J Biol Chem 2001;276:20813–20816. [PubMed: 11319214]

Shaw AS. Lipid rafts: now you see them, now you don't. Nat Immunol 2006;7:1139–1142. [PubMed: 17053798]

Shogomori H, Brown DA. Use of detergents to study membrane rafts: the good, the bad, and the ugly. Biol Chem 2003;384:1259–1263. [PubMed: 14515986]

Silvius J. Lipid microdomains in model and biological membranes: how strong are the connections? Q Rev Biophys 2005;38:373–383. [PubMed: 16600056]

Simons K, Ikonen E. Functional rafts in cell membranes. Nature 1997;387:569–572. [PubMed: 9177342]

Simons K, Vaz WL. Model systems, lipid rafts, and cell membranes. Annu Rev Biophys Biomol Struct 2004;33:269–295. [PubMed: 15139814]

Smith HG Jr, Litman BJ. Preparation of osmotically intact rod outer segment disks by Ficoll flotation. Methods Enzymol 1982;81:57–61. [PubMed: 7047994]

Sun H, Nathans J. Mechanistic studies of ABCR, the ABC transporter in photoreceptor outer segments responsible for autosomal recessive Stargardt disease. J Bioenerg Biomembr 2001;33:523–530. [PubMed: 11804194]

Sun H, Molday RS, Nathans J. Retinal stimulates ATP hydrolysis by purified and reconstituted ABCR, the photoreceptor-specific ATP-binding cassette transporter responsible for Stargardt disease. J Biol Chem 1999;274:8269–8281. [PubMed: 10075733]

Tan E, Wang Q, Quiambao AB, et al. The relationship between opsin overexpression and photoreceptor degeneration. Invest Ophthalmol Vis Sci 2001;42:589–600. [PubMed: 11222515]

Weng J, Mata NL, Azarian SM, Tzekov RT, Birch DG, Travis GH. Insights into the function of Rim protein in photoreceptors and etiology of Stargardt's disease from the phenotype in abcr knockout mice. Cell 1999;98:13–23. [PubMed: 10412977]

Wiegand RD, Koutz CA, Stinson AM, Anderson RE. Conservation of docosahexaenoic acid in rod outer segments of rat retina during n-3 and n-6 fatty acid deficiency. J Neurochem 1991;57:1690–1699. [PubMed: 1833510]

Wollscheid B, von Haller PD, Yi E, et al. Lipid raft proteins and their identification in T lymphocytes. Subcell Biochem 2004;37:121–152. [PubMed: 15376619]

Xu X, London E. The effect of sterol structure on membrane lipid domains reveals how cholesterol can induce lipid domain formation. Biochemistry 2000;39:843–849. [PubMed: 10653627]

Yu C, Alterman M, Dobrowsky RT. Ceramide displaces cholesterol from lipid rafts and decreases the association of the cholesterol binding protein caveolin-1. J Lipid Res 2005;46:1678–1691. [PubMed: 15863835]

Zacharias DA, Violin JD, Newton AC, Tsien RY. Partitioning of lipid-modified monomeric GFPs into membrane microdomains of live cells. Science 2002;296:913–916. [PubMed: 11988576]

Zhang X, Cote RH. cGMP signaling in vertebrate retinal photoreceptor cells. Front Biosci 2005;10:1191–1204. [PubMed: 15769618]

Zimmerman WF, Godchaux W III. Preparation and characterization of sealed bovine rod cell outer segments. Methods Enzymol 1982;81:52–57. [PubMed: 7047993]

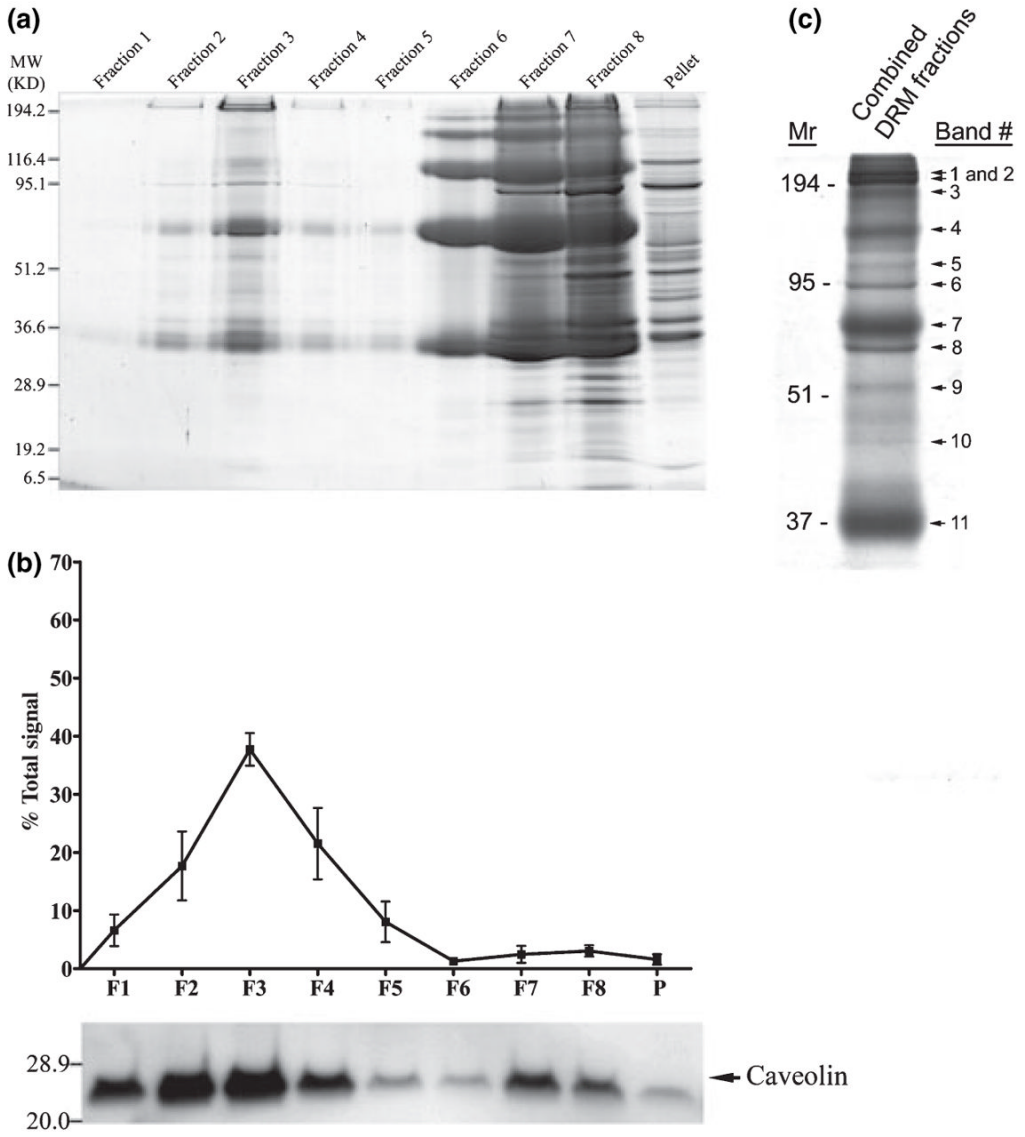

Fig. 1.

(a) Representative Coomassie blue-stained 12% SDS–PAGE gel of bovine ROS membrane fractions [F1–F8, and pellet (P)] obtained by Triton X-100 treatment and differential sucrose density-gradient ultracentrifugation. (b) Semi-quantitative western (immunoblot) analysis of the distribution of Cav-1 (upper panel) and a representative Cav-1 immunoblot (lower panel) of these membrane fractions. Migration positions of protein molecular weight markers are denoted by numbers on the left-hand side of the gel and blot. Cav-1 distribution was determined by densitometric analyses of blots; the amount in each fraction is plotted as a percent of the total Cav-1 in all the fractions (see Materials and methods). Error bars represent standard deviation (SD) of the mean percent in each fraction (N = 4 DRM fractionations, from 4 independent ROS preparations). (c) Coomassie blue-stained 12% SDS–PAGE gel of proteins from concentrated DRM fractions subsequently analyzed by mass spectrometry. Band numbers of excised bands subjected to mass spectrometric analysis are indicated to the right of the gel. These band numbers correspond to those indicated in Table 1.

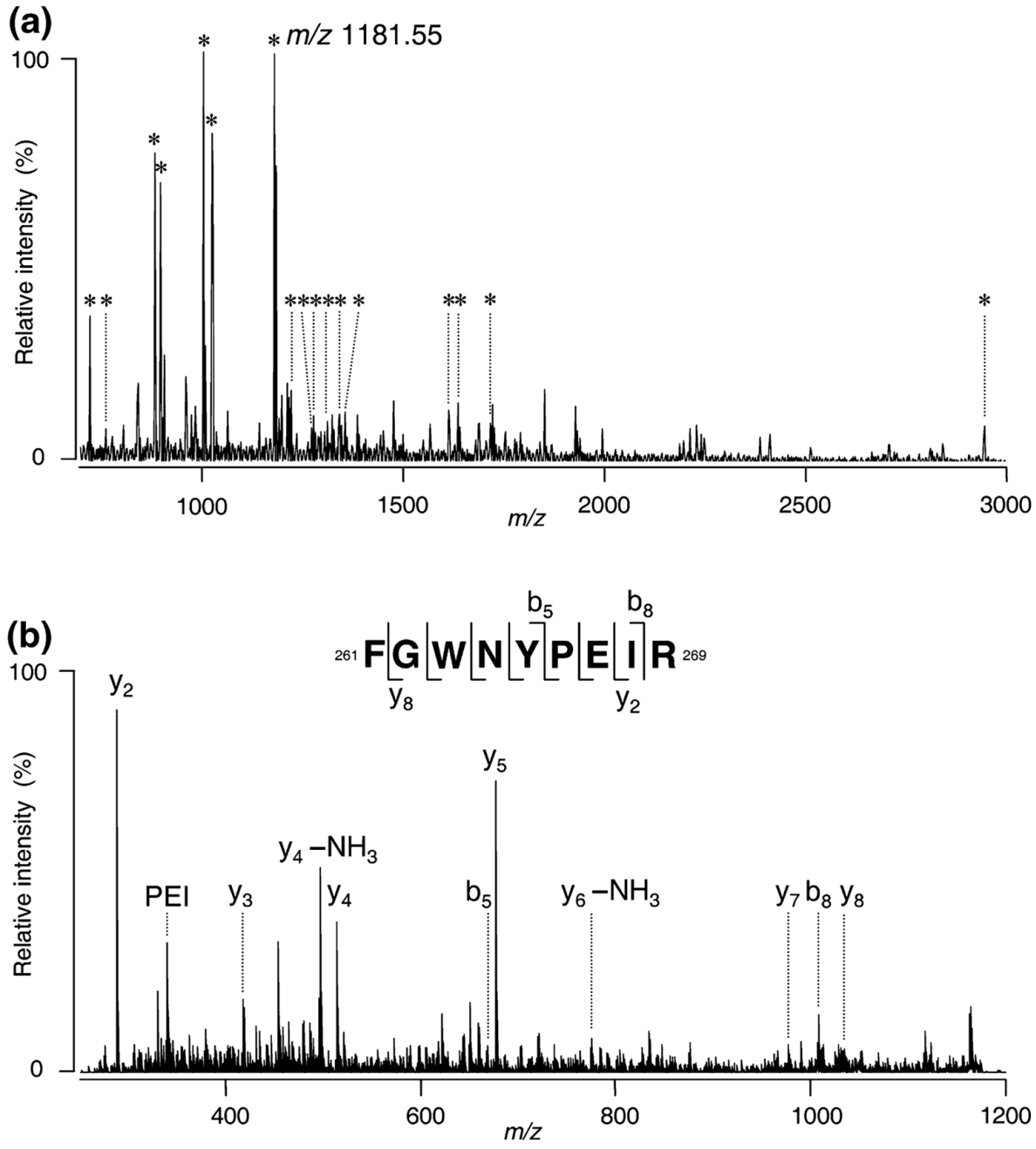

Fig. 2.

Characterization of tryptic peptides from bovine DRM proteins using MALDI-TOF mass spectrometry. (a) MS spectrum of the tryptic digests using MALDI-TOF. The peaks with the assigned m/z value consistent with the theoretical tryptic peptide mass of the candidate CNG-α1 subunit are indicated by the asterisks. (b) MS/MS spectrum of an ion peak at m/z 1181.55 (see panel a) using MALDI-QIT-TOF MS. The C-terminal y-series and N-terminal b-series ions derived from the peptide corresponded to the amino acid residues 261–269 of CNGα-1.

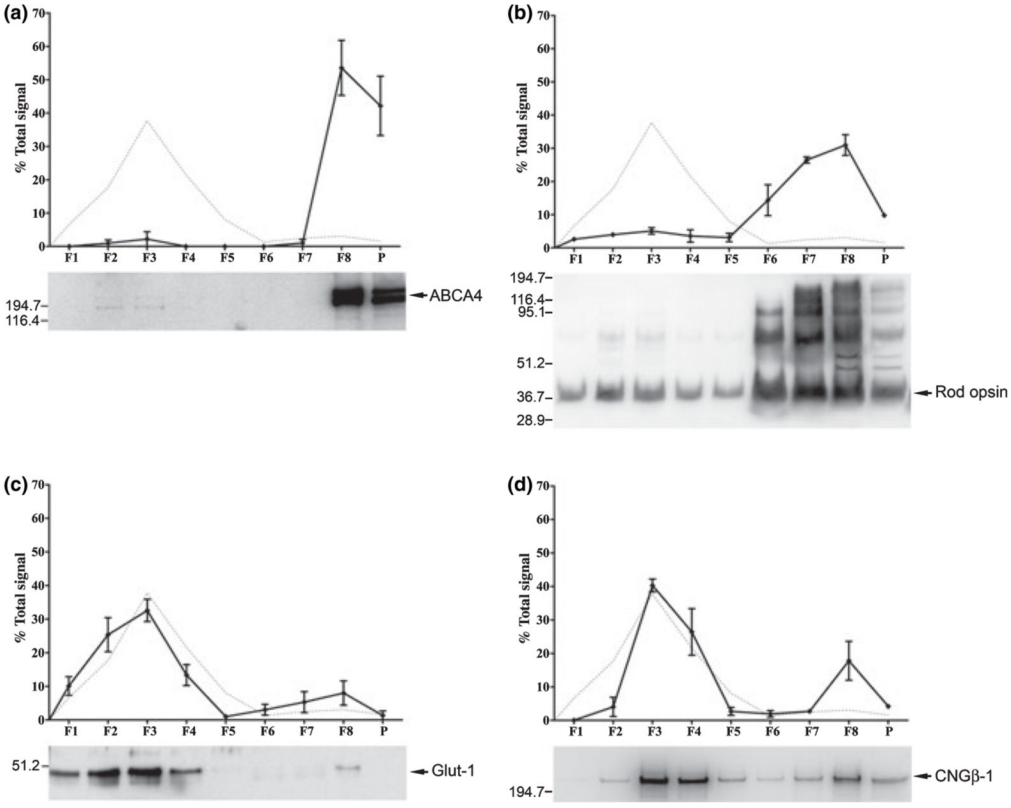

Fig. 3.

Semi-quantitative analysis of the fractionation of integral membrane proteins to ROS-derived DRMs. DRM fractions (F1–F4) contain only a small percentage of the total amount of ABCA4 (a), a somewhat higher percentage of rod opsin (b), and dramatic enrichment of Glut-1 (c) and CNG β-1 (d). In each case, the upper panels show the percentage of each protein (solid lines) plotted along with the distribution of Cav-1 (dashed lines, replotted from Fig. 1) to designate DRM fractions; lower panels show corresponding western blot. Error bars represent the SD of mean values obtained from four independent DRM preparations (from 4 separate ROS preparations).

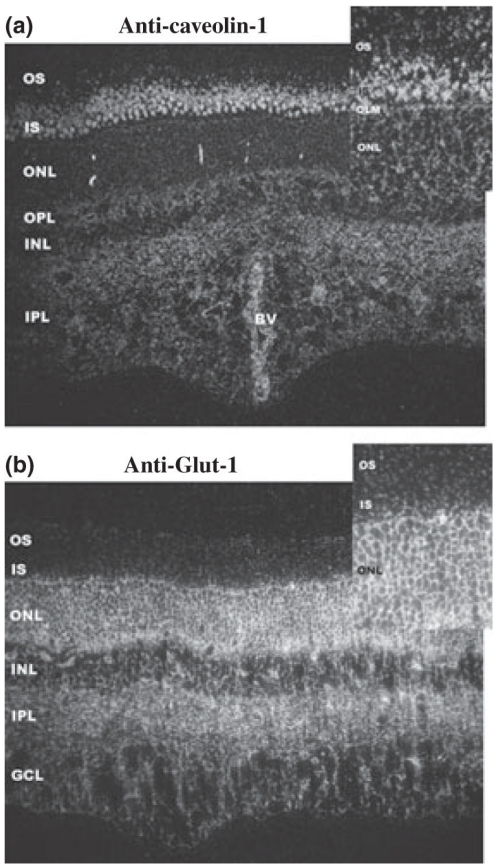

Fig. 4.

Dark-field, light microscopic, silver-enhanced immunogold labeling of bovine retina with antibodies against (a) Cav-1 and (b) Glut-1. In each, the inset panel represents a higher-magnification image. Note the minimal, diffuse labeling of the outer segment (OS) layer with both DRM-specific markers. Abbreviations: IS, inner segment layer; ONL, outer nuclear layer; OPL, outer plexiform layer; OLM, outer limiting membrane; INL, inner nuclear layer; IPL, inner plexiform layer; GCL, ganglion cell layer; BV, blood vessel. Scale bar (all panels): 25 μm.

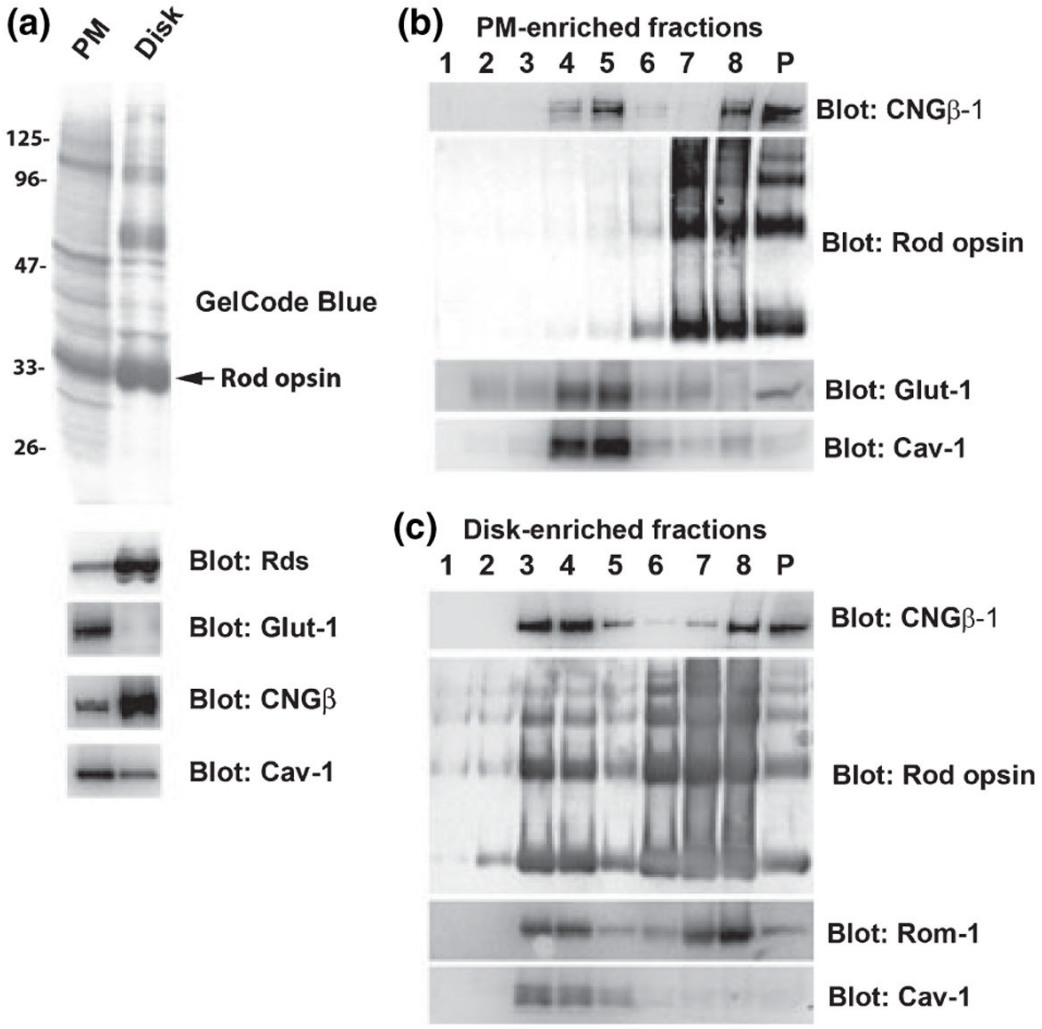

Fig. 5.

Isolation and characterization of DRM and non-DRM fractions from bovine ROS plasma membranes (PM) and disks. (a) Upper panel: GelCode Blue®-stained SDS–PAGE gel of isolated ROS PM and disk fractions. Lower panel: Corresponding western blots, probed with antibodies to disk marker proteins (CNGβ-1 and Rds), a PM marker protein in disks (Glut-1), and a DRM marker protein (Cav-1). (b) Western blot analysis of sucrose gradient fractions of DRMs prepared from ROS PM, probed with antibodies against CNGβ-1, rod opsin, Glut-1, and Cav-1. (c) Western blot analysis of sucrose gradient fractions of DRMs prepared from ROS disk membranes probed with antibodies against CNGβ-1, rod opsin, Rom-1, and Cav-1. Note that the DRM fraction distribution in PM is shifted to slightly heavier density (F4–F5), compared to the DRM fractions obtained from disk membranes (F3–F4).

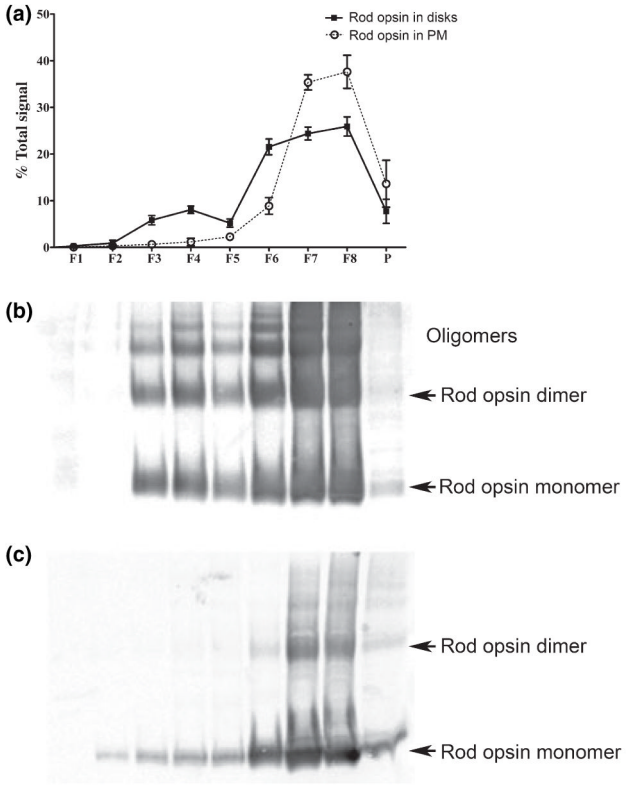

Fig. 6.

Semi-quantitative analyses of rod opsin distribution in DRM fractions derived from disk and PM-enriched membranes. (a) Distributions of rod opsin in DRM fractions from disks (filled squares/solid line) and PM (open circles/dotted line) were determined by densitometric analyses of blots from three independent DRM fractionations. The amount of rod opsin in each fraction is plotted as a percent of the total rod opsin in all the fractions. Error bars represent standard deviation (S.D.) of the mean percent in each fraction (N = 3 DRM fractionations each from three independent disk/PM isolations). Representative immunoblots from disk (b) and from PM (c) are also shown.

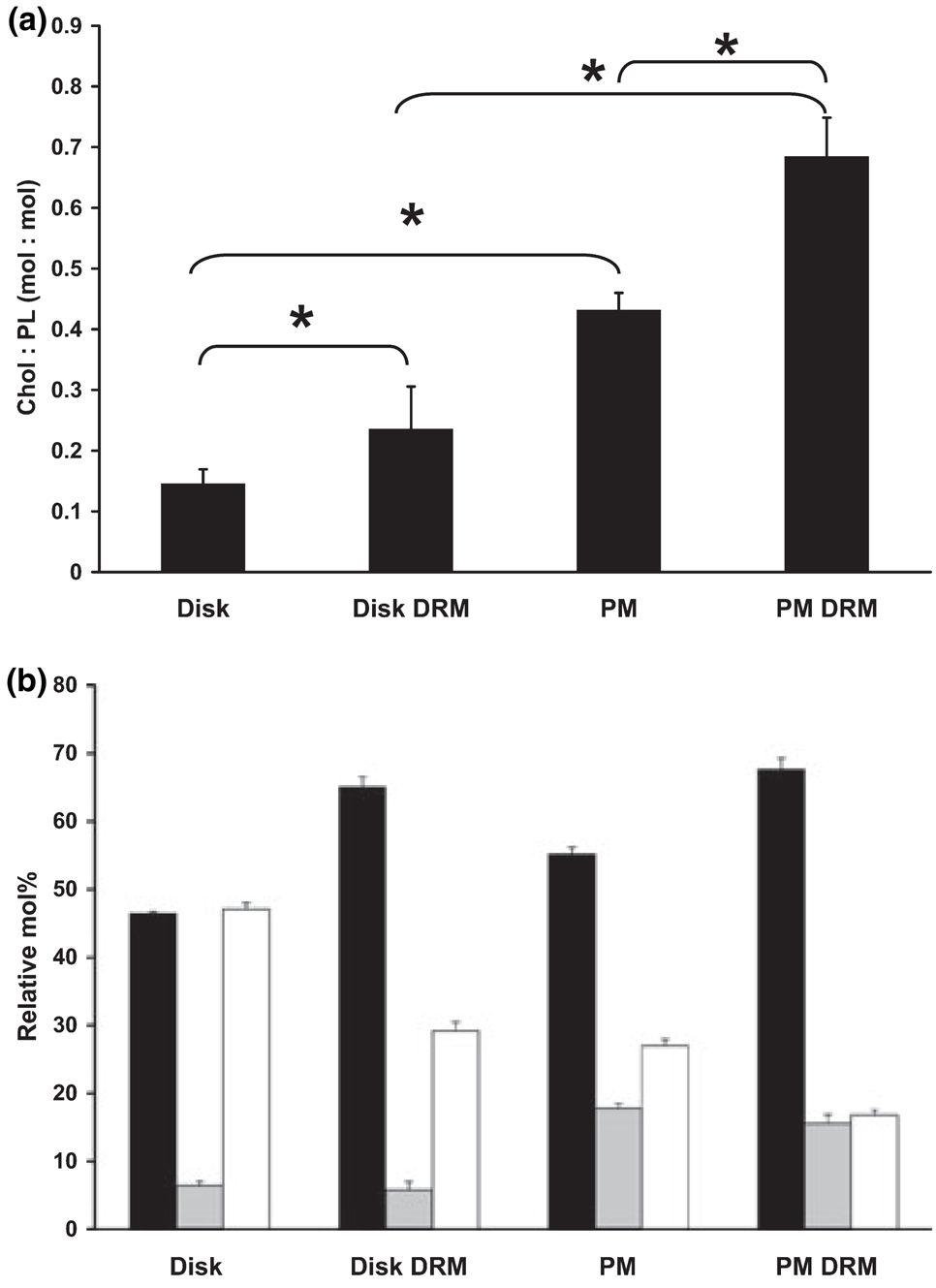

Fig. 7.

(a) Cholesterol/phospholipid (Chol: PL) mole ratio of unfractionated ROS disk membranes, disk DRMs, unfractionated ROS plasma membranes (PM), and PM-derived DRMs. (b) Correlative distribution (relative mol%) of saturated (black bars), monounsaturated (shaded bars), and polyunsaturated (open bars) fatty acids in each of the membrane fractions shown in panel a. Data represent mean values (with SD error bars), N = 3 independent preparations each. Asterisks (*) denoted statistically significant differences ($p < 0.05$).

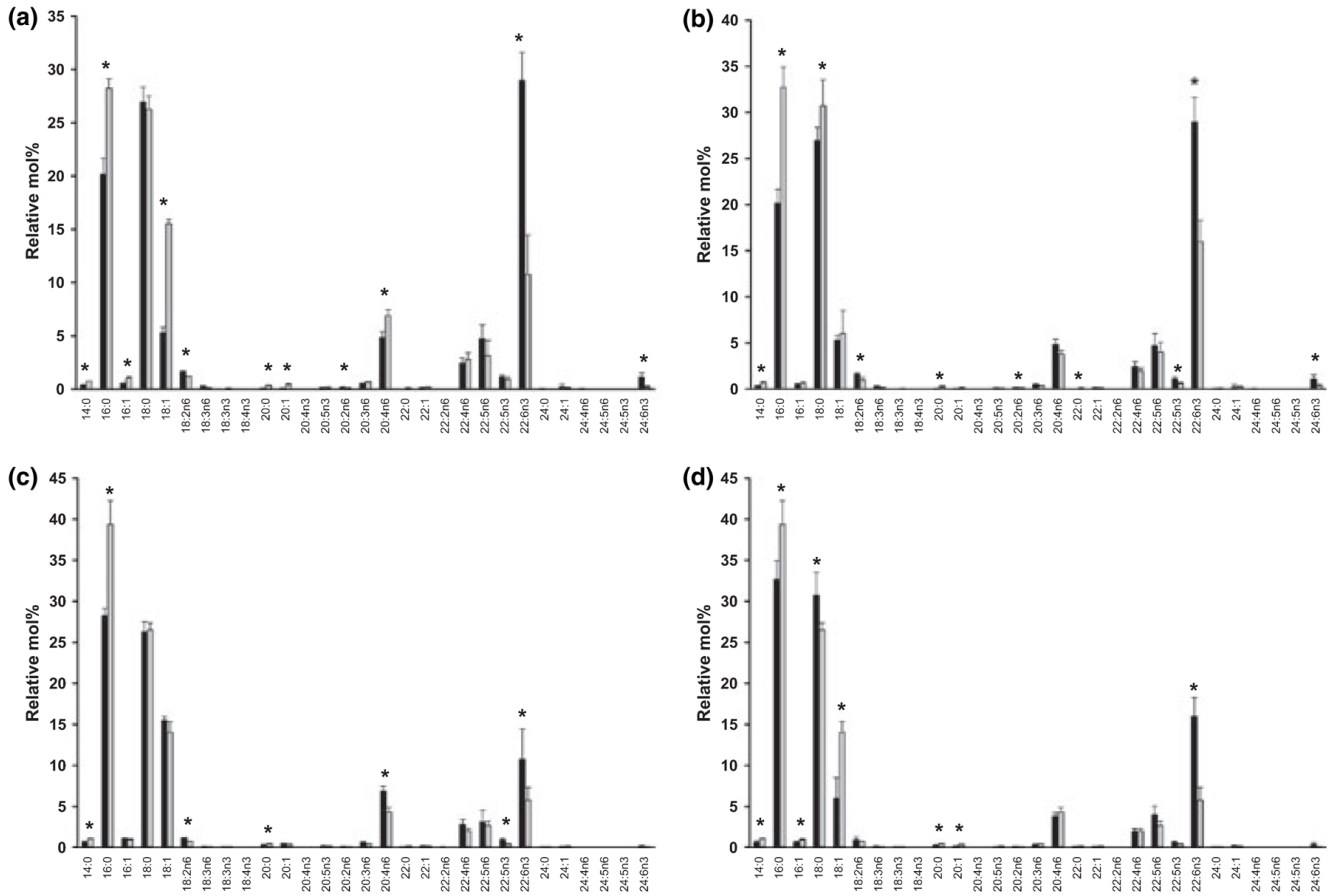

Fig. 8.

Comparative fatty acid composition analysis of ROS disk and PM fractions (mean values expressed as relative mol%, with SD; N = 3). (a) Disk membranes (black bars) vs. plasma membranes (shaded bars). (b) Unfractionated disk membranes (black bars) vs. disk DRMs (shaded bars). (c) Unfractionated plasma membranes (black bars) vs. plasma membrane DRMs (shaded bars). (d) Disk DRMs (black bars) vs. plasma membrane DRMs (shaded bars). Asterisks (*) denoted statistically significant differences ($p < 0.05$).

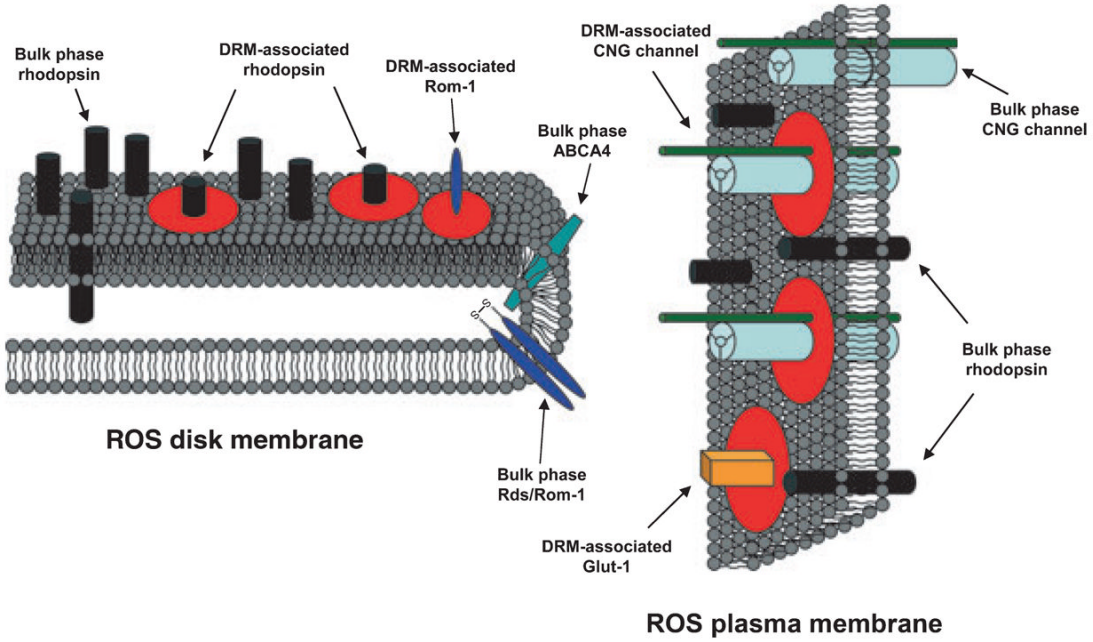

Fig. 9.

Schematic model depicting the segregation of ROS disk and PM proteins into DRM vs. non-DRM (bulk phase) domains. DRM domains are indicated by red circles. Rod opsin is entirely localized to the bulk phase in the ROS PM and is largely localized to the bulk phase in disk membranes, with a small portion residing in disk DRMs. Most Rom-1 and essentially all Rds and ABCA4 in the ROS are localized to non-DRM domains in disks; these proteins are not present in the ROS PM. The majority of CNG ion channels and essentially all Glut-1 transporters are localized to PM-derived DRMs; neither of these proteins is found in disks.

Table 1

List of identified proteins from ROS-derived DRM fractions

Band # in Fig. 1	Observed MW (kDa)[a]	Protein[b]	Theoretical MW/pI	NCBI Accession #	PMF MOWSE score[c]	Sequence coverage (%)[d]	MS/MS MOWSE score[e]	MS/MS[f]
1	200	ATP-binding cassette, sub-family A, member 4, bovine	260049/5.9	27806343	159	11	50	2
2	200	Cyclic nucleotide-gated channel beta 1, bovine	106771/5.0	3309626	151	18	45	3
3	190	ATP-binding cassette, sub-family A, member 4, bovine	260049/5.9	27806343	167	18	56	3
4	116	Rhodopsin, bovine	39692/5.9	62460472	51	9	45	2
5	97	Na+/K+-ATPase alpha 3 subunit, bovine	103207/5.2	61816544	75	10	42	2
6	95	Cyclic GMP phosphodiesterase (rod receptor), alpha polypeptide, bovine	100311/5.3	48675838	99	24	53	3
6	95	Cyclic GMP phosphodiesterase (rod receptor), beta polypeptide, bovine	99759/5.2	27806057	74	20	64	3
7	75	Rhodopsin, bovine	39692/5.9	62460472	70	14	50	2
8	70	Cyclic nucleotide-gated channel alpha 1, bovine	80049/6.7	27805875	71	22	49	3
9	52	ATPase, H+ transporting, lysosomal 56/58 kDa, V1 subunit B, isoform 2, bovine	56917/5.4	28603810	84	15		
10	39	Solute carrier family 2, member 1 (glucose transporter type 1), bovine	54523/8.9	27807089	74	13	42	3
11	37	Rhodopsin, bovine	39692/5.9	62460472	74	17	50	2

[a] Apparent molecular weights of protein bands observed in SDS–PAGE.

[b] Names of identified proteins in MS and/or MS/MS analysis.

[c] MOWSE scores of peptide mass fingerprinting (PMF) analysis provided by the MASCOT program. Scores ≥69 represent $p < 0.05$.

[d] Coverage of amino acid sequence by peptide mass fingerprinting analysis.

[e] MOWSE scores of MS/MS analysis provided by the MASCOT program. Scores ≥40 represent $p < 0.05$.

[f] Number of peptides used in MS/MS analysis.